NOAA Technical Report NESDIS 85

CALIBRATION OF THE ADVANCED MICROWAVE SOUNDING UNIT-A FOR NOAA-K

Washington, D.C.
June 1995

U.S. DEPARTMENT OF COMMERCE
National Oceanic and Atmospheric Administration
National Environmental Satellite, Data, and Information Service

NOAA TECHNICAL REPORTS

National Environmental Satellite, Data, and Information Service

The National Environmental Satellite, Data, and Information Service (NESDIS) manages the Nation's civil Earth-observing satellite systems, as well as global national data bases for meteorology, oceanography, geophysics, and solar-terrestrial sciences. From these sources, it develops and disseminates environmental data and information products critical to the protection of life and property, national defence, the national economy, energy development and distribution, global food supplies, and the development of natural resources.

Publication in the NOAA Technical Report series does not preclude later publication in scientific journals in expanded or modified form. The NESDIS series of NOAA Technical Reports is a continuation of the former NESS and EDIS series of NOAA Technical Reports and the NESC and EDS series of Environmental Science Services Administration (ESSA) Technical Reports.

A limited number of copies are available by contacting Nancy Everson, NOAA/NESDIS, E/RA22, 5200 Auth Road, Washington D.C., 20233. Copies can also be ordered from the National Technical Information Service (NTIS), U.S. Department of Commerce, Sills Bldg., 5285 Port Royal Road, Springfield, VA. 22161, (703) 487-4650 (prices on request for paper copies or microfiche, please refer to PB number when ordering). A partial listing of more recent reports appear below:

NESDIS 26 Monthly and Seasonal Mean Outgoing Longwave Radiation and Anomalies. Arnold Gruber, Marylin Varnadore, Phillip A. Arkin and Jay S. Winston, October 1987. (PB87 160545/AS)

NESDIS 27 Estimation of Broadband Planetary Albedo from Opertional Narrowband Satellite Measurements. James Wydick, April 1987. (PB88 107644/AS)

NESDIS 28 The AVHRR/HIRS Operational Method for Satellite Based Sea Surface Temperature Determination. Charles Walton, March 1987. (PB88 107594/AS)

NESDIS 29 The Complementary Roles of Microwave and Infrared Instruments in Atmospheric Soundings. Larry McMillin, February 1987. (PB87 184917/AS)

NESDIS 30 Planning for Future Operational Sensors and Other Priorities. James C. Fischer, June 1987. (PB87 220802/AS)

NESDIS 31 Data Processing Alogorithms for Inferring Stratospheric Gas Concentrations from Balloon-Based Solar Occultation Data. I-Lok Chang (American University) and Michael P. Weinreb, April 1987. (PB87 196424)

NESDIS 32 Precipitation Detection with Satellite Microwave Data. Yang Chenggang and Andrew Timchalk, June 1988. (PB88 240239)

NESDIS 33 An Introduction to the GOES I-M Imager and Sounder Instruments and the GVAR Retransmission Format. Raymond J. Komajda (Mitre Corp) and Keith McKenzie, October 1987. (PB88 132709)

NESDIS 34 Balloon-Based Infrared Solar Occultation Measurements of Stratospheric 03, H20, HNo3, and CF2C12. Michael P. Weinreb and I-Lok Chang (American University), September 1987. (PB88 132725)

NESDIS 35 Passive Microwave Observing From Environmental Satellites, A Status Report Based on NOAA's June 1-4, 1987, Conference in Williamsburg, VA. James C. Fisher, November 1987. (PB88 208236)

NESDIS 36 Pre-Launch Calibration of Channels 1 and 2 of the Advanced Very High Resolution Radiometer. C. R. Nagaraja Rao, October 1987. (PB88 157169/AS)

NESDIS 39 General Determination of Earth Surface Type and Cloud Amount Using Multispectral AVHRR Data. Irwin Ruff and Arnold Gruber, February 1988. (PB88 199195/AS)

NESDIS 40 The GOES I-M System Functional Description. Carolyn Bradley (Mitre Corp), November 1988.

NESDIS 41 Report of the Earth Radiation Budget Requirements Review - 1987, Rosslyn, VA, 30 March-3 April 1987. Larry L. Stowe (Editor), June 1988.

NESDIS 42 Simulation Studies of Improved Sounding Systems. H. Yates, D. Wark, H. Aumann, N. Evans, N. Phillips, J. Sussking, L. McMillin, A. Goldman, M. Chahine and L. Crone, February 1989.

NESDIS 43 Adjustment of Microwave Spectral Radiances of the Earth to a Fixed Angle of Progagation. D. Q. Wark, December 1988. (PB89 162556/AS)

NESDIS 44 Educator's Guide for Building and Operating Environmental Satellite Receiving Stations. R. Joe Summers, Chambersburg Senior High, February 1989.

NESDIS 45 Final Report on the Modulation and EMC Consideration for the HRPT Transmission System in the Post NOAA-M Polar Orbiting Satellite ERA. James C. Fisher (Editor), June 1989. (PB89 223812/AS)

NESDIS 46 MECCA Program Documentation. Kurt W. Hess, September 1989.

NESDIS 47 A General Method of Using Prior Information in a Simultaneous Equation System. Lawrence J. Crone, David S Crosby and Larry M. McMillin, October 1989.

NOAA Technical Report NESDIS 85

CALIBRATION OF THE ADVANCED MICROWAVE SOUNDING UNIT-A FOR NOAA-K

Tsan Mo
Office of Research and Applications
Satellite Research Laboratory
Physics Branch

Washington, D.C.
June 1995

U.S. DEPARTMENT OF COMMERCE
Ronald H. Brown, Secretary

National Oceanic and Atmospheric Administration
D. James Baker, Under Secretary

National Environmental Satellite, Data, and Information Service
Robert S. Winokur, Assistant Administrator

CONTENTS

Table Captions

FIGURE CAPTIONS

CALIBRATION OF THE ADVANCED MICROWAVE SOUNDING UNIT-A FOR NOAA-K

Tsan Mo
NOAA/NESDIS
Office of Research and Applications
Satellite Research Laboratory
Washington, D. C. 20233

ABSTRACT

The thermal-vacuum chamber calibration data from the Advanced Microwave Sounding Unit-A (AMSU-A) for NOAA-K, which will be launched in 1996, were analyzed to evaluate the instrument performance, including calibration accuracy, nonlinearity, and temperature sensitivity. The AMSU-A on NOAA-K consists of AMSU-A2 Protoflight Model and AMSU-A1 Flight Model 1. The results show that both models meet the instrument specifications, except the AMSU-A1 antenna beamwidths, which exceed the requirement of 3.3°±10%. We also studied the instrument's radiometric characterizations which will be incorporated into the operational calibration algorithm for processing the in-orbit AMSU-A data from space. Particularly, the nonlinearity parameters which will be used for correcting the nonlinear contributions from an imperfect square-law detector were determined from this data analysis. It was found that the calibration accuracies (differences between the measured scene radiances and those calculated from a linear two-point calibration formula) are polarization-dependent. Channels with vertical polarizations show little cold biases at the lowest scene target temperature 84K, while those with horizontal polarizations all have appreciable cold biases, which can be up to 0.6K. It is unknown where these polarization-dependent cold biases originate, but it is suspected that some chamber contamination of hot radiances leaked into the cold scene target area. Further investigation in this matter is required. The existence and magnitude of nonlinearity in each channel were established and a quadratic formula for modeling these nonlinear contributions was developed. The model was characterized by a single parameter u, values of which were obtained for each channel via least-squares fit to the data. Using the best-fit u values, we performed a series of simulations of the quadratic corrections which would be expected from the space data after the launch of AMSU-A on NOAA-K. In these simulations, the cosmic background radiance corresponding to a cold space temperature 2.73K was adopted as one of the two reference points of calibration. The largest simulated nonlinear correction is about 0.3K, which occurs at channel 15 when the instrument temperature is at 38.09° C. Others are less than 0.2K in the remaining channels. Possible improvement for future instrument calibration is also discussed.

1. INTRODUCTION

AMSU-A is a new generation of total-power microwave radiometers, consisting of 15 channels in two separate units: AMSU-A2 with two channels at 23.8 and 31.4 GHz; and AMSU-A1 with 12 channels in the range of 50.3 to 57.290344 GHz plus one channel at 89.0 GHz. Totally, AMSU-A1 furnishes 13 channels (channels 3 through 15) using two antenna systems, A1-1 and A1-2. The 12 oxygen-band channels (Channels 3-14) will provide the microwave temperature sounding for regions from the Earth's near-surface to about 42 kilometer (km), or from 1000 to 2 millibars (mb). The remaining three "window" channels (Channels 1, 2, and 15) will aid the temperature sounding by correcting for the surface emissivity, atmospheric liquid water, and total precipitable water. These window channels also provide information on precipitation, sea ice, and snow coverage. Each of the AMSU-A antenna systems requires to have a nominal field-of-view (FOV) 3.3° at the half-power points and to cover a crosstrack scan of ±48° 20' (to beam centers) from the nadir direction with 30 Earth FOVs per scan line. Beam positions 1 and 30 are the extreme scan positions of the Earth views, while beam positions 15 and 16 are near the nadir direction. Onboard blackbody and cold space calibrations will be performed once every 8 seconds for each scan line.

Three AMSU-A flight models, i.e., Protoflight Model (PFM), Flight Model 1 (FM1) and Flight Model 2 (FM2) have been built by GenCorp/Aerojet Electronic Systems Division, the AMSU-A contractor. Two additional flight models will be built within the next few years. These AMSU-A instruments will be flown aboard the NOAA-K, L, M, N, and N' spacecrafts, which constitute a new generation of Polar-orbiting Operational Environmental Satellites (POES). The first AMSU-A instrument is scheduled for launch in 1996 on NOAA-K, which will be renamed as NOAA-15 after launch. This follows the tradition that a NOAA spacecraft is named by an alphabetical letter before launch after which, a numerical series number replaces its letter nomenclature. The AMSU-A on NOAA-K consists of AMSU-A2 PFM and AMSU-A1 FM1.

Each of the flight models were tested and calibrated in a thermal-vacuum (T/V) chamber by Aerojet. After Aerojet completes its contractual obligations, the calibration data are transferred to NOAA for evaluation. NOAA scientists analyze and evaluate these test data to determine the instrument's radiometric characterizations which will be incorporated into the operational calibration algorithm for processing the in-orbit AMSU-A data. Particularly, the nonlinearity parameters which will be used in the AMSU-A calibration algorithm for correcting the nonlinear contributions from an imperfect square-law detector must be extracted from this pre-launch calibration.

The present study was undertaken to analyze and evaluate the T/V chamber test data from the first set of AMSU-A instruments, which will be launched aboard NOAA-K in 1996. We also developed an analytic formula that can be used to simulate quantitatively the magnitude of the nonlinearity contributions to the radiometric temperatures expected in space. The same formula was used in an earlier report [1] for studying the calibration data from the AMSU-A Engineering Model, but it was further extended in this study to the region of cold space radiance (corresponding to 2.73K) for explicitly simulating the nonlinearity corrections at three instrument temperatures for each channel.

In the following sections, we present the results of our data analysis. Specification topics evaluated in this analysis include calibration accuracy, nonlinearity, and radiometric temperature sensitivity (or NEΔT, the noise-equivalent temperature). Section 1 gives an introduction and section 2 presents a brief description of the T/V chamber test data. The calibration algorithm is described in section 3 and results are presented in section 4. Conclusion and discussion are given in section 5, where several issues related to improve future instrument calibration are discussed. The procedures of calculating the warm load correction factor and its results are described in Appendix A, which also lists the channel characteristics and the measurement errors of the calibration data. Tables of coefficients, which will be used in the operational processing software, are given in Appendix B. A brief description of the NOAA Polar Orbiter Level 1B data is given in Appendix C.

2. DESCRIPTION OF DATA

All data used in this report were taken by Aerojet in its T/V test chamber using the full scan mode. In this mode, AMSU-A scans through 30 scene-view (or beam) positions, the cold target, and the internal warm blackbody target once every 8 seconds. It takes one look (or sample) at each beam position and two looks at the cold and warm targets, respectively. Since the scene calibration target was fixed at beam position 6 (31°40' from nadir), only radiometric counts from the beam position 6 can be used for calibration. Each antenna system looks at its own individual cold, warm, and scene targets, temperatures of which are measured by Platinum Resistance Thermometers (PRTs). The numbers of PRTs used to measure the physical temperatures of the scene, cold, and warm calibration targets in each antenna system are given in Table 1, which also lists the channels provided by each AMSU-A antenna system. Channels 9-14 have both primary and secondary phase locked loop oscillators (called PLLO#1 and PLLO#2, respectively) built-in. The PLLO#2 will be used for backup if PLLO#1 fails. Invar high-Q cavity stabilized local osillators [7] are used in other channels.

Table 1. Number of PRTs in each calibration target and channels provided by individual antenna systems. The last row gives the number of scans collected in the calibration for each system.

Items	AMSU Antenna Systems			Remarks
	A2	A1-2	A1-1	
PRTs in Warm Target	7	5	5	See Note 1
PRTs in Cold Target	11	7	7	See Note 2
PRTs in Scene Target	11	7	7	
Channels	1 & 2	3, 4, 5 & 8	6, 7, & 9-15	
PLLO#2	-	-	Ch. 9-14	Backup PLLO
N(Scan NO.)	120	400 to 900	400 to 900	See Note 3

Notes: 1. Warm Load PRT #1 in A1-1 is bad.
2. Cold Target PRT #609 in A1-2 is bad.
3. For A1-1 & A1-2: N=400, 400, 550, 725, 725, and 900 when the scene target temperature T_s=84, 130, 180, 230, 280, and 330K, respectively.

It should be noted that one of the PRTs in AMSU-A1-1 Warm Target did (will) not work and that another PRT in the AMSU-A1-2 Cold Target was also bad. These two PRTs were excluded in obtaining the temperatures from the individual targets.

The physical temperatures of scene and cold targets measured by individual PRTs were provided in Kelvin (K) on Aerojet's data tape. However, the signals from the PRTs monitoring the warm blackbody targets are given in counts, which are proportional to the blackbody temperatures. One should note that the scene and cold targets used in the T/V chamber will not be carried into space. The PRT counts from warm blackbody targets must be converted to PRT temperatures. The normal approach of deriving the PRT temperatures from counts is a two-step process: (1) the resistance of each PRT in ohms is computed by a count-to-resistance look-up table provided by the manufacturer. In this study, we used a polynomial representation of the count-to-resistance relationship provided by Aerojet; and (2) the individual PRT temperature in degrees Celsius is obtained from an analytic PRT equation, which is described in Appendix B. However, the two steps can be compressed to a

single step with negligible errors. This single step process, which will be used in operation, computes the PRT temperatures directly from the PRT counts, using a cubic polynomial

$$T_k = \sum_{j=0}^{3} f_{kj} C_k^j \tag{1}$$

where T_k and C_k represent the temperature and count of the PRT k. The polynomial coefficients, f_{kj}, are obtained for each PRT. Equation (1) also applies to 47 other housekeeping temperature sensors, such as the mixers, the IF amplifiers and the local oscillators. These f_{kj} coefficients for all PRTs and housekeeping sensors in AMSU-A1 FM1 and AMSU-A2 PFM are listed in Appendix B (Tables B-1 and B-2, respectively).

The mean internal blackbody temperature, T_w, is calculated from the individual PRT temperatures,

$$T_w = \frac{\sum_{k=1}^{m} w_k T_k}{\sum_{k=1}^{m} w_k} + \Delta T_w \tag{2}$$

where m represents the number of PRTs for each antenna system (as listed in Table 1) and w_k is a weight assigned to each PRT. The quantity ΔT_w is a warm load correction factor, which will be derived for each channel from the T/V test data at three instrument temperatures (extreme low, nominal, and extreme high). The ΔT_w values for each AMSU-A antenna system are given in Appendix A. The w_k value, which equals 1 (0) if the PRT k is determined good (bad) before launch, will be provided for each flight model. In this study, we set w_1=0 for the PRT #1 in AMSU-A1-1, since it was (and will remain) bad (see Table 1), but all other PRTs have w_i = 1.

Similarly, the mean temperatures of scene and cold targets are defined in the same way as in Equation (2), except without the term ΔT_w. As shown in Table 1, one of the cold target PRTs in AMSU-A1-2 is bad and was excluded (by setting its w_i=0) in this study.

The T/V calibration data were taken at three instrument temperatures and the scene target was sequenced through six temperatures 84, 130, 180, 230, 280, and 330K, respectively, at each instrument temperature. At each of the scene target temperatures, calibration data were acquired for a number of scans to assure an effective temperature sensitivity less than 0.03K. The number of

scans required depends upon the expected NEΔT of channel 14 (which has the largest NEΔT) and is therefore a function of the scene target temperature. Actual numbers of scans taken at individual temperatures are given in Table 1. The uncertainties in knowledge of brightness temperatures and measurement errors were obtained by Aerojet. These are given in Appendix A.

Antenna beamwidths at all channels were also measured and the values are listed in Table A-2. One should note that beamwidths for AMSU-A1 channels exceed the 3.3°±10% specification. The largest deviation occurs at channel 15 and its measured value is 3.80°. Therefore, the surface resolution will be proportionally larger than the originally specified 48 km at nadir. Antenna beam efficiency at each channel frequency is greater than 95% and Table A-2 lists the calculated values.

3. CALIBRATION ALGORITHM

In this study, radiometric measurements and variables related to the calibration process are given in radiance with dimension of mW/(m^2-sr-cm^{-1}), instead of temperature. This is necessary because all other instruments flown on NOAA satellites produce measurements in radiance. Conversion between brightness temperature and radiance was performed using the full Planck function (not the Rayleigh-Jeans approximation). This also eliminates any possible conversion inaccuracy that may occur, particularly in the region of the space cosmic back-ground temperature (~2.73K).

For each scan, the blackbody radiometric counts C_w are the averages of two samples of the internal blackbody. Similarly, the space radiometric counts C_c are the average of two samples of the space target. To reduce noise in the calibrations, the C_x (where x=w or c) for each scan line were convoluted over several neighboring scan lines according to a weight function [2]

$$\overline{C_x} = \frac{1}{n+1} \sum_{i=-n}^{n} \left(1 - \frac{|i|}{n+1} \right) C_x(t_i) \qquad (3)$$

where t_i (when $i \neq 0$) represents the time of the scan lines just before or after the current scan line. If t_0 is the time of the current scan line, one can write $t_i = t_0 + i\Delta t$, where $\Delta t = 8$ seconds for AMSU-A. The 2n+1 values are equally distributed about the scan line to be calibrated. Following the study of AMSU-A Engineering Model [1], the value of n=3 is chosen for all AMSU-A antenna systems. This produces the seven weights of 0.25, 0.5, 0.75, 1.0, 0.75, 0.5, and 0.25, respectively, from the weight factor that is defined within the parentheses in Equation (3) for the seven scans i = -3, -2, -1, 0, 1, 2, and 3.

In an earlier report [1], a calibration algorithm, which takes into account the nonlinear contributions due to an imperfect square-law detector, was employed to convert scene counts to scene radiances. The same calibration algorithm is used in this study to obtain the scene radiance R_s, given by

$$R_s = R_w + (R_w - R_c)\left(\frac{C_s - \overline{C_w}}{\overline{C_w} - \overline{C_c}}\right) + Q \quad , \qquad \frac{mW}{m^2\text{-}sr\text{-}cm^{-1}} \tag{4}$$

where R_w and R_c are the radiances computed from the PRT blackbody temperature T_w and the PRT cold target temperature T_c, respectively, using the Planck function. The C_s is the radiometric count from the scene (Earth) target. The averaged blackbody and space counts, $\overline{C_w}$ and $\overline{C_c}$, are defined by Equation (3). The quantity Q, which represents the nonlinear contribution, is given by [1]

$$Q = u\,(R_w - R_c)^2 \frac{(C_s - \overline{C_w})(C_s - \overline{C_c})}{(\overline{C_w} - \overline{C_c})^2} \tag{5}$$

where u is a free parameter, values of which are determined at three instrument temperatures (extreme low, nominal, and extreme high) that will be discussed in Section 5. The u values at other instrument temperatures will be interpolated from these three values. For channels 9-14 (AMSU-A1-1), two sets of the u parameters are provided; one set is for the primary PLLO#1 and the other one for the redundant PLLO#2.

The quantity R_s defined in Equation (4) represents the radiometric scene radiances observed at individual channels. For users of NOAA Level 1B data, a simplified formula, which converts C_s directly into R_s, is presented in Appendix C. It should be noted that the ratios in Equations (4) and (5) will eliminate (or reduce) the effect of any channel gain variation on R_s. The gain, G, of a channel is defined as

$$G = \frac{\overline{C_w} - \overline{C_c}}{R_w - R_c} \quad , \qquad \frac{Count \bullet (m^2\text{-}sr\text{-}cm^{-1})}{mW} \tag{6}$$

The quantity G varies with instrument temperature, which is defined as the RF Shelf temperature for each AMSU-A antenna system. For a fixed instrument temperature, G is approximately constant. The first two terms in Equation (4) constitute a linear two-point calibration equation, if the quadratic term is negligible. Let R_{sL} denote these two terms,

$$R_{sL} = R_w + (R_w - R_c)\left(\frac{C_s - \overline{C_w}}{\overline{C_w} - \overline{C_c}}\right) \quad , \qquad \frac{mW}{m^2 - sr - cm^{-1}} \tag{7}$$

We first calculate the radiometric scene radiances R_{sL} from the T/V chamber test data, using this two-point calibration equation. The results are given in Section 4.

4. RESULTS

4.1 *Calibration Accuracy*

The "calibration accuracy" is defined as the difference between the PRT scene radiance R_{sprt} (temperature) and the radiometric scene radiance (brightness temperature) with measured target emissivity of ~0.9999. It is calculated from the equation

$$\Delta R = \frac{1}{N}\sum_{i=1}^{N}\left(R_{sprt} - R_{sL}\right)_i \tag{8}$$

where N is the number of scans at individual scene temperatures (N= 120 for AMSU-A2 channels but ranging from 400 to 900 for AMSU-A1 channels).

Equation (7) would be a good representation of the microwave radiometric scene radiance from a perfect square-law detector. Any deviation of the quantity R_{sL} from the measured scene radiance R_{sprt} may indicate the presence of either nonlinearity in the system or some contamination of the calibration data from the T/V chamber. Figure 1 shows the calculated calibration accuracies versus the PRT scene radiances (R_{sprt}) for channels 1 through 15. The quantities along the ordinates on the left-hand side of these plots represent the calculated ΔR values from Equation (8), while the corresponding differences in temperature, ΔT (K), are shown on the right-hand side. The PRT scene temperatures, T_{sprt}, ranging from 84K (the lowest data point) to 330K (the highest data point) are plotted on the upper abscissas. The specification of AMSU-A instruments requires $\Delta T = 2.0K$ for channels 1, 2, and 15, and $\Delta T = 1.5K$ for all other channels. The results in Figure 1 show that the specifications are met at all channels.

It is interesting to note that the plots in Figure 1 appear in two distinct patterns. Those in channels 1, 2, 3, 4, 7, and 15 show little (or very small) ΔR values at the lower end of the PRT scene radiance (which corresponds to the lowest scene temperature 84K), while the remaining channels (5, 6, and

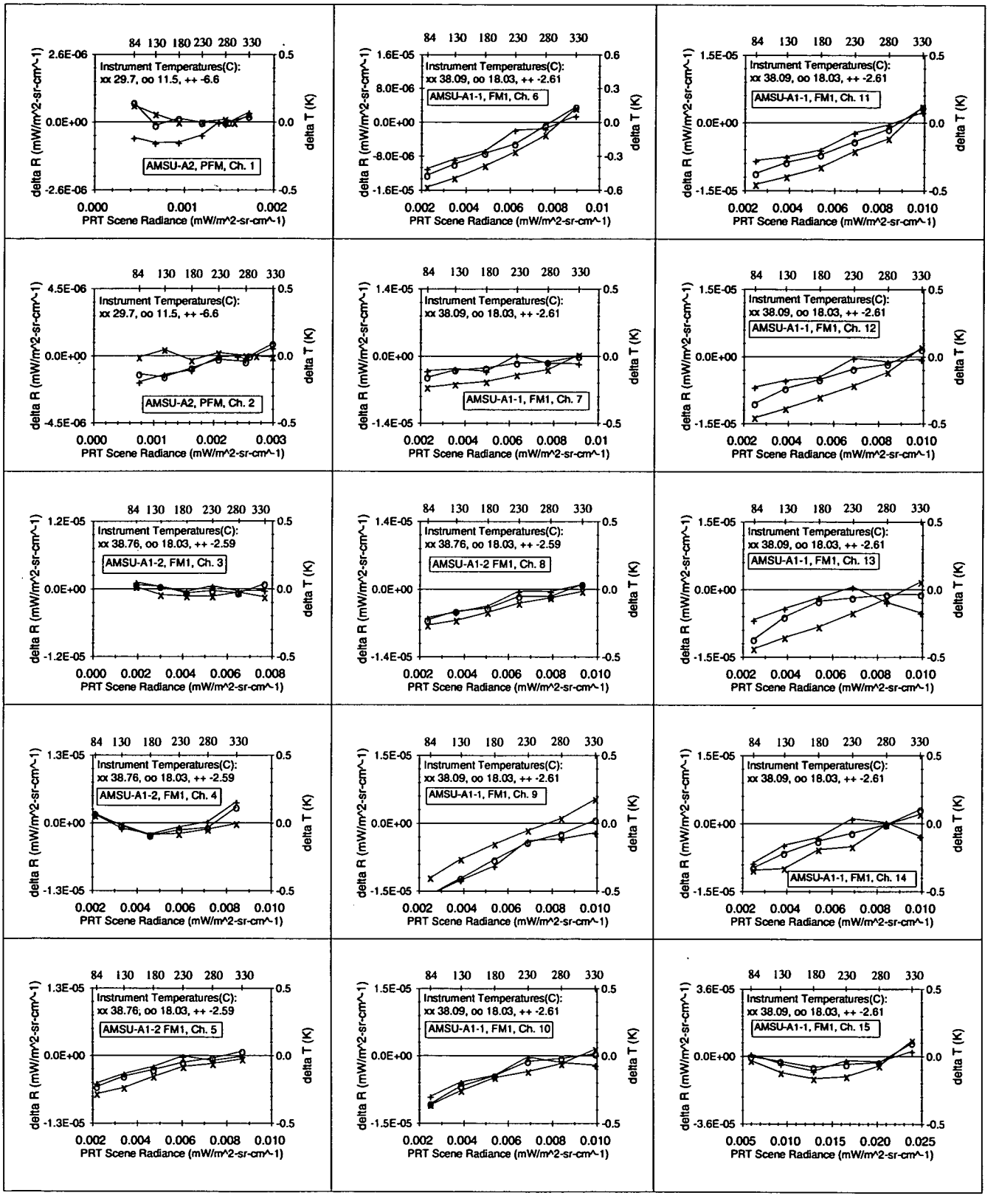

Figure 1. Calibration accuracies delta R versus PRT scene radiances for channels 1-15 at three instrument temperatures. The corresponding values in brightness temperature deltaT are given at the right-hand sides and the PRT scene temperatures are on the top. Note that the pattern of curves at the vertically polarized channels (1-4, 7 and 15) differs from the one of other channels, which are horizontally polarized.

8-14) have relatively large ΔR values or "cold biases," which can be up to 0.5K in most channels. The former group of channels all have vertical polarizations and the latter have horizontal polarizations. It is not well understood how these polarization-dependent cold biases originate. Inspection of the plots in Figure 1 shows that the magnitude of these cold biases becomes larger in most cases when the difference between the scene target temperature and instrument temperature increases. For example, in the case of channel 11 (Figure 1), the cold bias values are -0.28, -0.37, and -0.45K, respectively, when the instrument temperatures are at -2.61, 18.03, and 38.09° C. This suggests that there might be some hot "contamination" leaking into the regions of scene/cold targets in the T/V chamber and that some extra counts were resulted in the radiometric system.

4.2 *Nonlinearity*

The residual patterns at channels 4 and 15 (Figure 1) show clearly the nonlinearity forms which can be represented by the quadratic formula Q defined in Equation (5). Patterns at other channels are not so obvious because of the presence of cold biases. The nonlinearity of a channel is normally related to the residuals from a least-squares fit of its PRT scene radiances as a linear function of the radiometric radiances R_{sL} calculated from Equation (7). The nonlinearity can be calculated from the average of the differences (or residuals) between the R_{sprt} and the best-fit results from a linear equation in the form LinFit = $a + bR_{sL}$ (where a and b are the intercept and slope). These averaged residuals, which are denoted by Q (= R_{sprt} - LinFit) are shown in Figure 2. The largest (absolute) Q value on each curve is defined as its nonlinearity.

The plots in Figure 2 show that the maximum (absolute) Q values are about 0.1K, which can be observed at channels 1, 4, 6, 9, 10, 11, 13, 14, and 15, respectively. One should compare the results in Figure 2 with the AMSU-A specification, which requires Q = 0.5K for channels 1, 2, and 15; and Q = 0.375K for other channels. The results in Figure 2 show that the specifications are met at all channels. Most of the curves in Figure 2 have two roots and can be easily fitted by a quadratic equation, which can be written in the form

$$Q = u(R_s - R_1)(R_s - R_2) \tag{9}$$

where R_1 and R_2 represent the two roots. One can obtain a similar equation from Equation (5) by replacing the counts by its individual radiances, since the radiometric counts are proportional to radiances in a first-order approximation. The resultant equation represents a different straight line

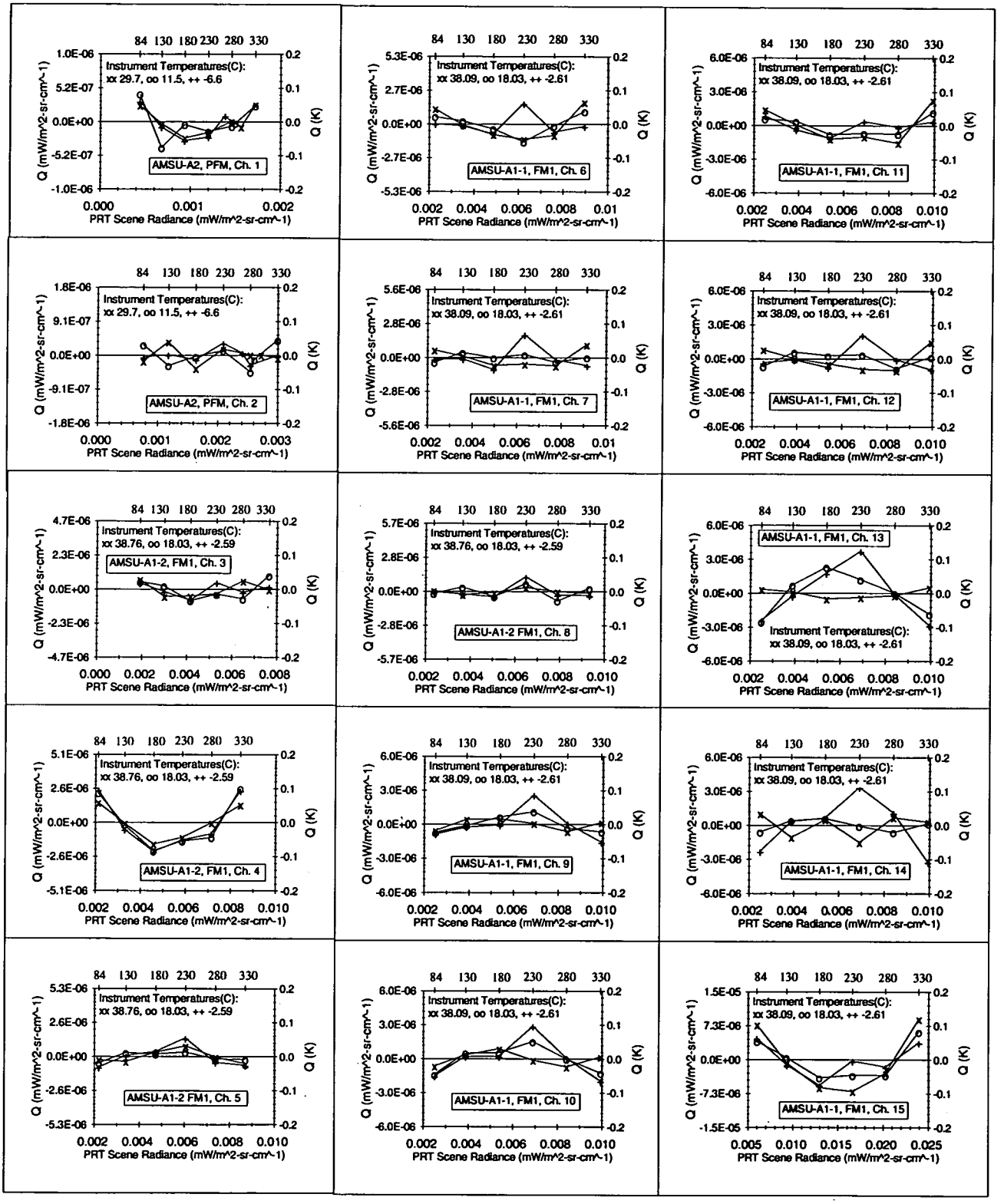

Figure 2. Residuals after a linear least-squares fit of the PRT scene radiances as a function of RsL, as defined in Eq. (7). These plots show the nonlinearities of the system. The largest (absolute) value on each curve represents the measured nonlinearity. One should note that all these residual values are less than the specifications, which are Q= 0.5K for channels 1, 2, and 15, and Q = 0.375K for other channels.

intersecting the same curve at R_w and R_c. Once the parameter u is determined, it can be used with any pair of roots to calculate Q. We applied Equation (9) to fit the quadratic curves in Figure 2 for obtaining the u values with the two roots extracted from each plot. Table 2 gives the best-fit u values at three instrument temperatures for individual channels.

Figure 3 show the residuals between the Q values (Figure 2) and the calculations from Equation (9) using the best-fit u values from Table 2. Inspection of the plots in Figure 3 reveals that the largest residuals after the quadratic fits are in the order of 0.05K (most are less than this).

4.3 Simulation of Quadratic Corrections to Space Data

Once the u values are determined, Equation (9) can be used to simulate the quadratic contributions which are expected from in-orbit data. This can be accomplished by replacing the roots R_1 and R_2 with the radiances $R_{2.73}$ (corresponding to cold space temperature 2.73K) and R_w, respectively. The simulated results are shown in Figure 4 for all channels at three instrument temperatures which are listed in the plots. One should note that the instrument temperatures are slightly different for the three AMSU-A antenna systems. The simulated quadratic contributions displayed in Figure 4 are larger than those shown in Figure 2. This is expected because the separation of the two reference calibration points is increased in the cases of simulations. Figure 4 shows that there are little nonlinearities at channels 5 and 8 and that a very small magnitude of contribution (~ 0.02K) appears in channel 3. Noticeable quadratic contributions appear at other channels. The largest one occurs at channel 15 and has a magnitude of 0.3K at the extreme high instrument temperature 38.09° C. Also, channels 4, 6, 10, 11, 12, 13, and 14 have nonlinearities with magnitude between 0.1 and 0.2K, while the remaining ones are less than 0.1K. It is important to point out that the effects of instrument temperature on the quadratic contributions are nonlinear for most channels.

Similarly, Figure 5 shows the calculated results which are associated with the redundant PLLO#2 built into channels 9-14. The upper half of Figure 5 (similar to Figure 1) displays the calibration accuracies, while the bottom half (similar to Figure 4) shows the simulated quadratic corrections which would be expected from in-orbit data. Comparison of the plots in Figure 5 (bottom part) with the corresponding ones in Figure 4 shows that the quadratic patterns have close similarities, except in case of channel 14.

Table 2. Values of the nonlinearity parameter u obtained from least-squares fit to data at three instrument tempeatures. The u has a dimension of (m^2-sr-cm^-1)/mW.

AMSU-A2 Channels: **AMSU-A1-2 Channels:**

Instrument Temperature (C)	CH. 1	CH. 2	Instrument Temperature (C)	CH. 3	CH. 4	CH. 5	CH. 8
29.7	1.109810	-0.050246	38.76	0.048428	0.269246	-0.013142	-0.009438
11.5	1.128380	0.309354	18.03	0.080626	0.439102	-0.003414	0.001171
-6.6	0.980173	-0.072332	-2.59	0.055511	0.444932	-0.027906	-0.000369

AMSU-A1-1 Channels: (PLLO #1)

Instrument Temperature (C)	CH. 6	CH. 7	CH. 9	CH. 10	CH. 11	CH. 12	CH. 13	CH. 14	CH. 15
38.09	0.232594	0.112400	-0.022126	-0.029466	0.220561	0.139549	0.044524	0.021492	0.188672
18.03	0.087373	-0.015400	-0.047238	-0.169687	0.020415	-0.025818	-0.284480	-0.022299	0.103593
-2.61	-0.010790	-0.000626	-0.148429	-0.239106	0.075740	-0.082410	-0.353876	-0.371479	0.092549

AMSU-A1-1 Channels: (PLLO #2)

Instrument Temperature (C)	CH. 9	CH. 10	CH. 11	CH. 12	CH. 13	CH. 14
38.77	0.049806	0.016424	0.174105	0.035468	0.001316	-0.063196
16.95	-0.085951	-0.130501	0.123357	0.011045	-0.136397	-0.010211
-2.12	-0.155463	-0.170186	0.168389	-0.052939	-0.250147	-0.024656

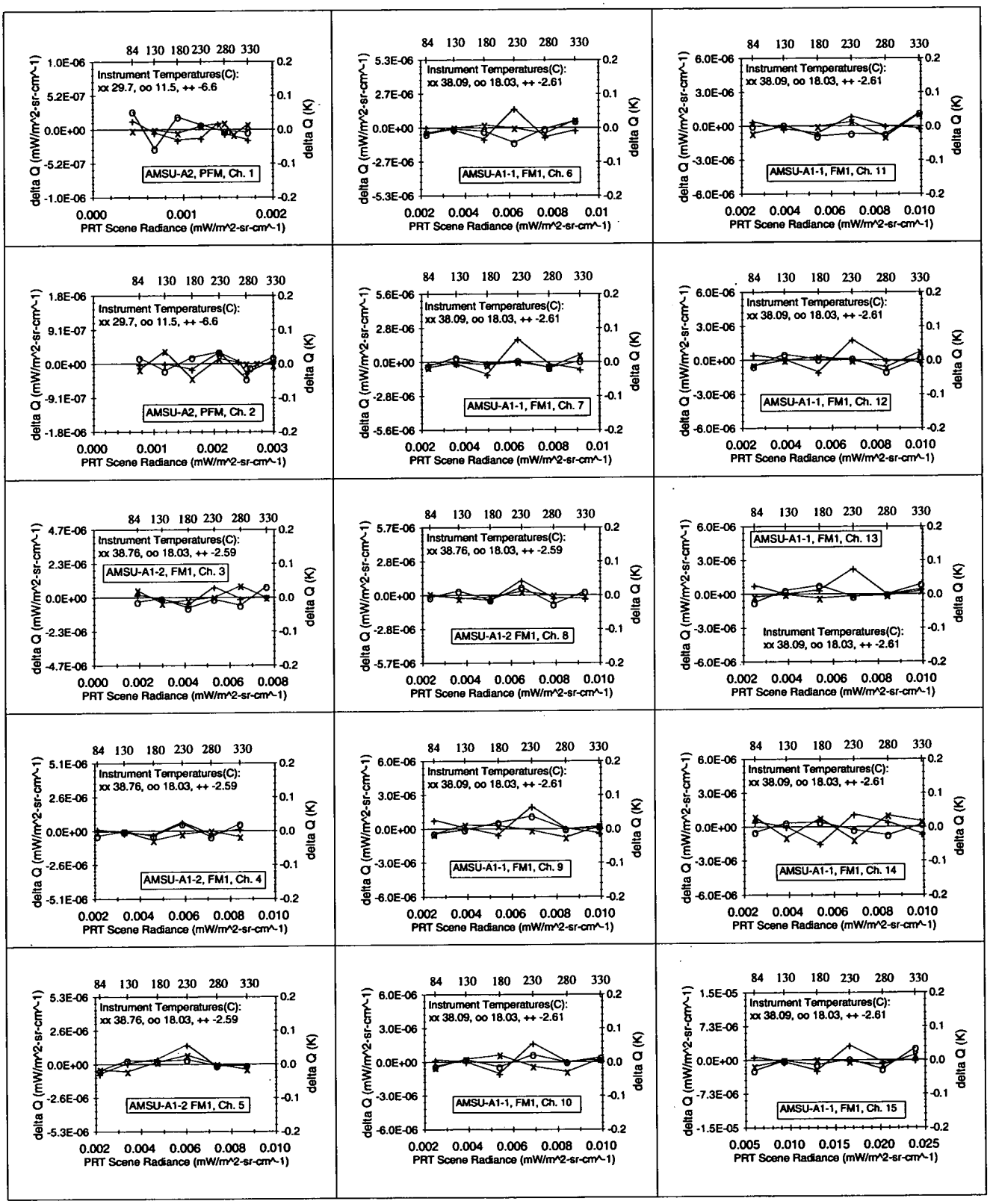

Figure 3. Residuals after applying the quadratic fits. Details are described in Section 4.

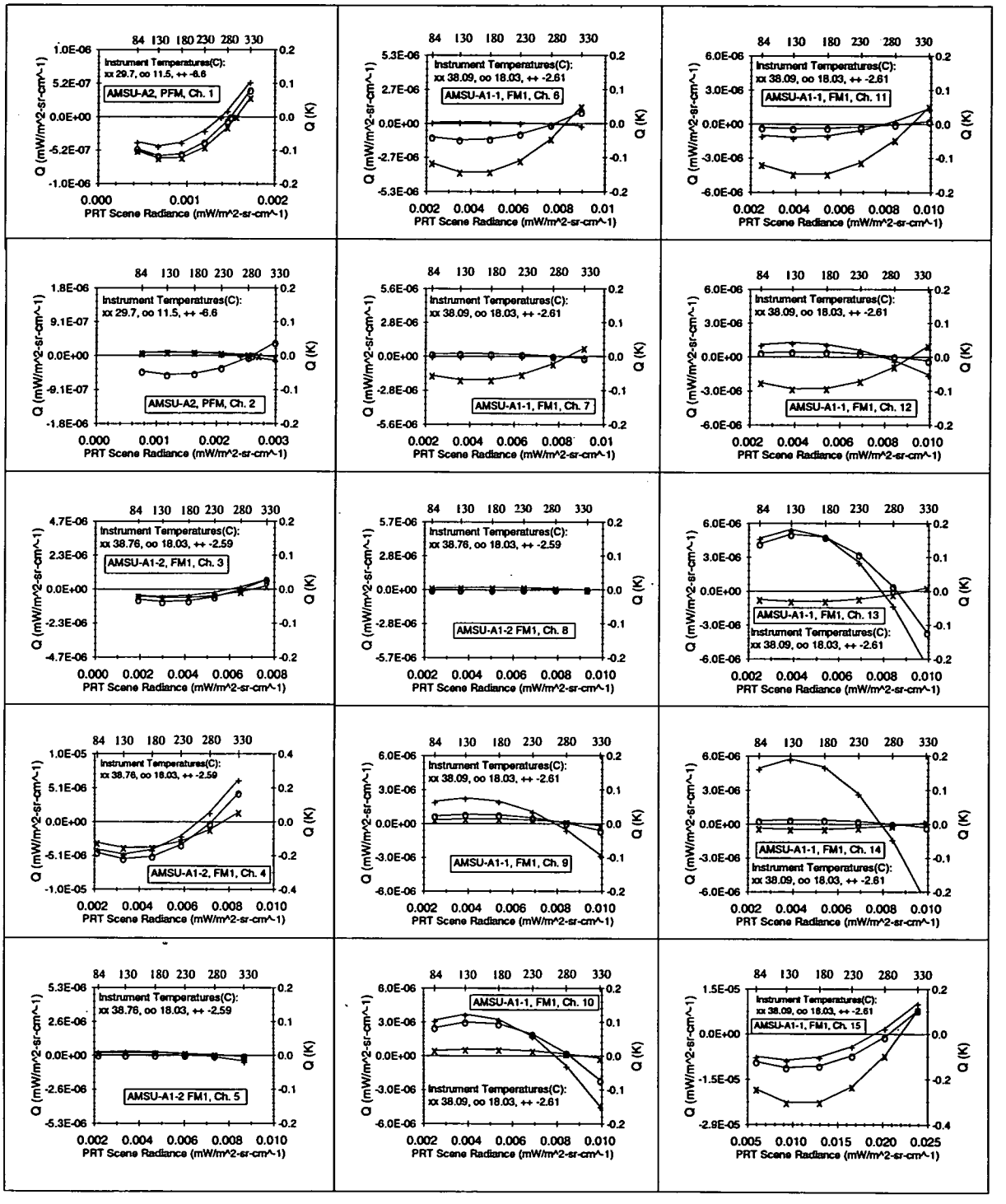

Figure 4. Simulated nonlinear corrections which would be expected from in-orbit data. Note that the effects of instrument temperature on the quadratic contributions for most channels are nonlinear.

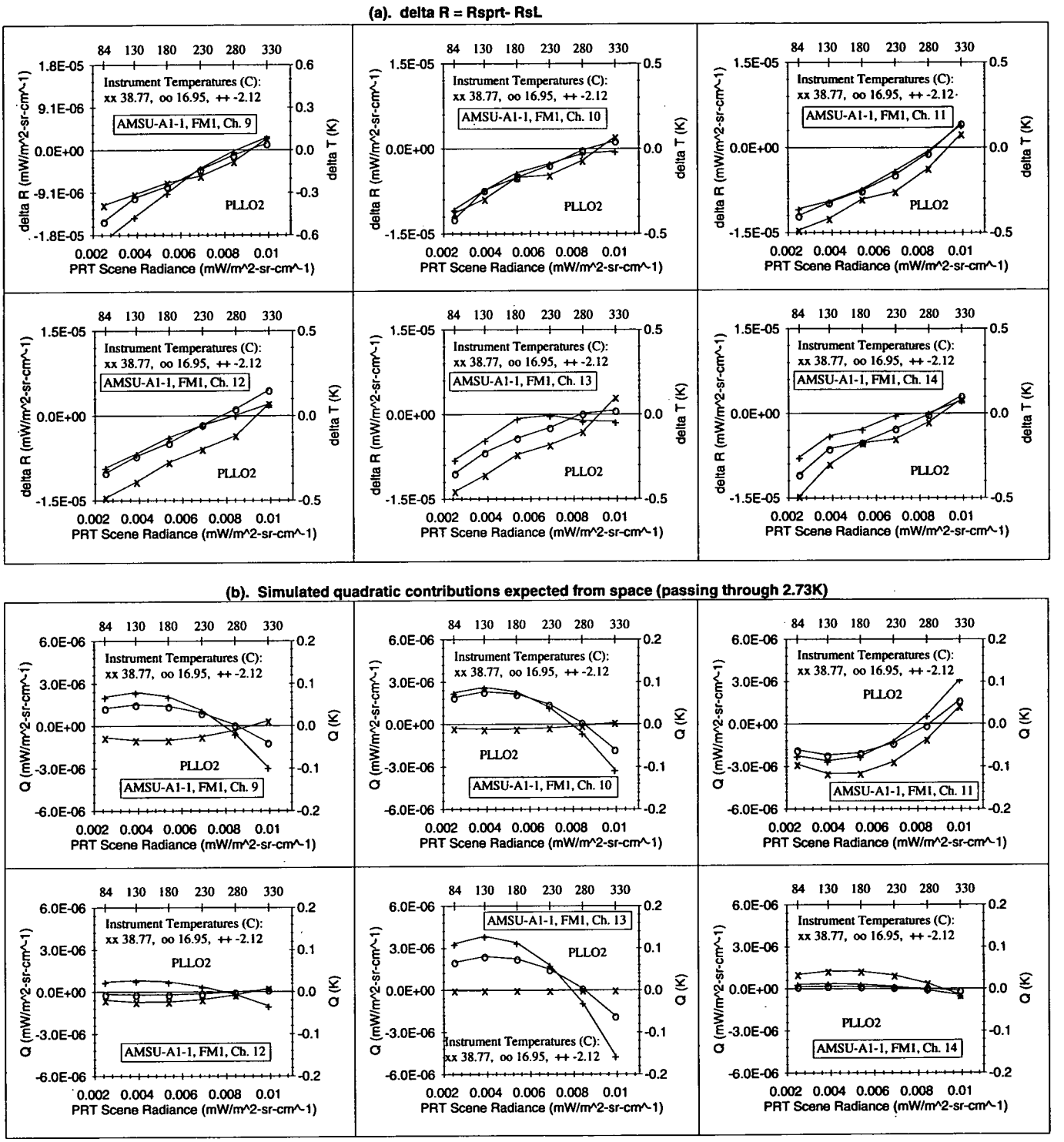

Figure 5. (a). Calibration accuracy: delta R versus PRT scene radiances with the PLLO#2 in channels 9-14. Others are the same as Figure 1.

(b). Simulated nonlinear corrections which will be expected from in-orbit data with PLLO#2 in channels 9-14. Others are same as Figure 4.

4.4 Temperature Sensitivity

The temperature sensitivity (or NEΔT) requirements for AMSU-A channels are listed in Table A-2. It is defined as the minimum change of scene brightness temperature that can be detected. In practice, it is calculated as the standard deviation of the radiometer output (in K), when an antenna system is viewing a scene target at 300K. The calculated NEΔT values are shown in Figure 6 together with the requirements from the AMSU-A specifications. These calculated NEΔT values (see Table A-2) correspond to a scene temperature of 305K, because they are the mean values of two measurements taken at the scene target temperatures of 280K and 330K, respectively (no calibration data were taken at 300K). All of the calculated NEΔT values in Figure 6 are less than those given in the AMSU-A specification [4]. Actually, all NEΔT values measured at both 280 and 330K satisfy the specification.

4.5 Radiometric Counts at Zero Radiance

Figure 7 shows nine sample plots of radiometric counts versus the PRT temperatures taken from the AMSU-A1-1 channels. The radiometric counts consist of cold counts at 84K, scene counts with scene temperatures ranging from 84 to 330K, and warm counts at the warm target temperatures (~300K), respectively. The number of data points (at each PRT temperature) in Figure 7 varies from N = 400 at 84K to 900 at 330K (see Table 1). These data points coincide to each other and cannot be distinguished in the plots. Each symbol x represents all of these data points (not averaged value). Figure 7 shows that good linear relationships exist between the radiometric counts and the PRT temperatures in the range 84 to 330K. We can extrapolate these linear relationships to 0K (corresponding to zero radiance) and obtain the intercepts for these plots. The intercept for each data point can also be computed from Equation (7) by setting R_{sL}= 0 and solve for C_s, which is denoted by C_{sint}. Then we have

$$C_{sint} = \overline{C_w} - G R_w \qquad (10)$$

where G is the channel gain defined in Equation (6). The calculated C_{sint} values at three instrument temperatures for each channel are listed in Table 3. These are the mean values of all calculations performed with all available calibration data (from 400 to 900 scans as the scene temperature varies from 84 to 330K). At each instrument temperature, the variation in the calculated C_{sint} values is relatively small and all C_{sint} values are positive. These C_{sint} values are associated with the system

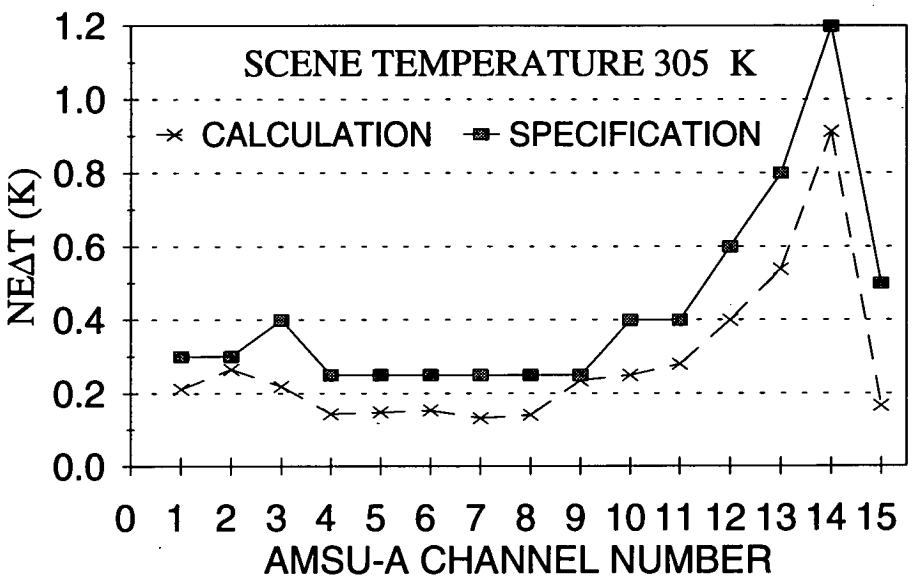

Figure 6. Comparison of the calculated (measured) NEdT values to the specifications. Note that all calculated ones are smaller than the specifications.

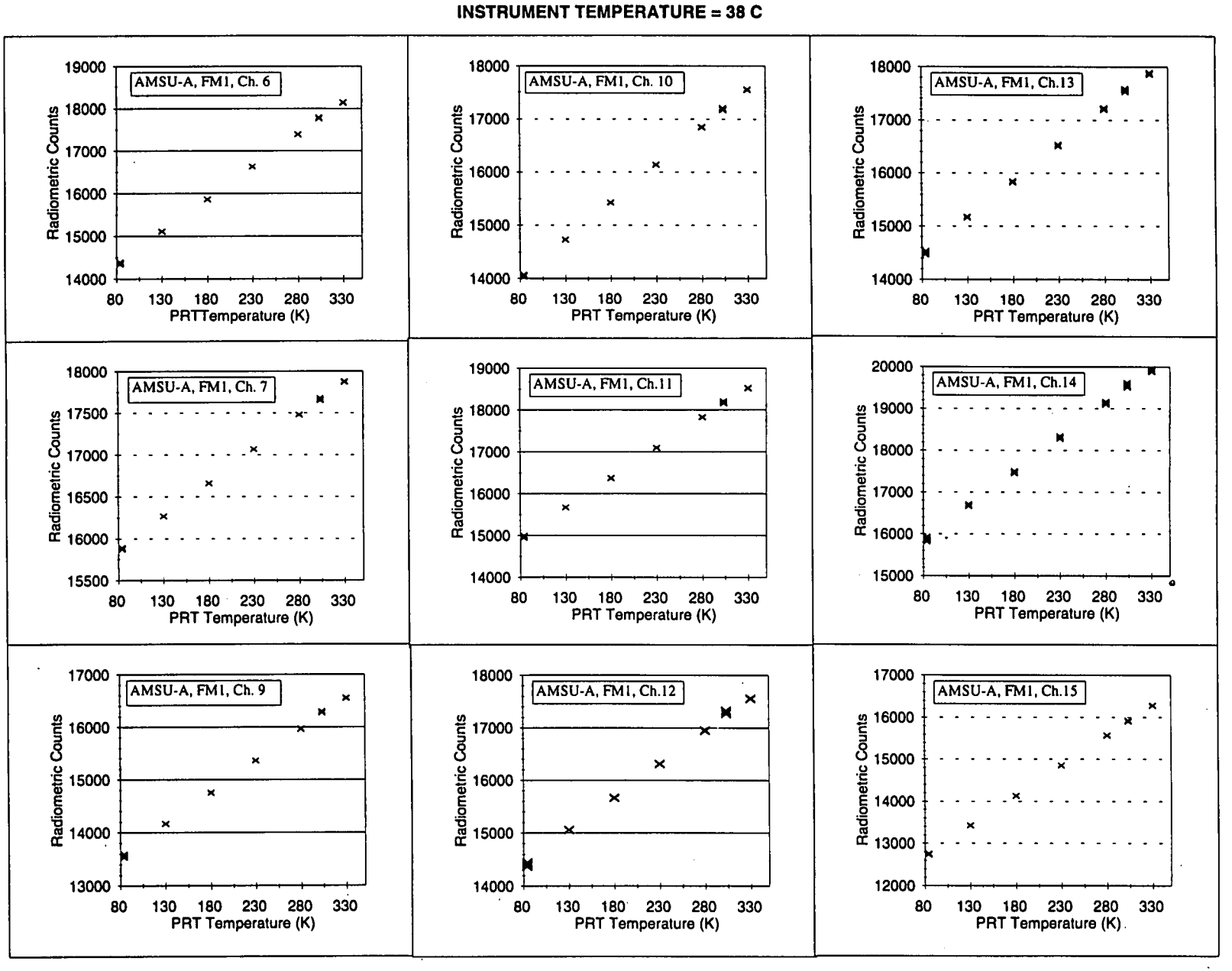

Figure 7. Radiometric counts versus PRT temperatures. Note that the cold and warm counts are near 84K and 300K, respectively. The thickness of the x's represents variation of the data.

Table 3. Radiometric counts at zero radiances. Equation (10) was used to obtain these values as described in the text.

AMSU-A2 Channels: AMSU-A1-2 Channelks:

Instrument Temp. (C)	Scene Temp. (K)	Ch 1	Ch 2	Instrument Temp. (C)	Scene Temp. (K)	Ch 3	Ch 4	Ch 5	Ch 8
29.50	84.02	12983	13421	38.72	83.86	12370	12907	10188	10363
29.33	129.89	12984	13428	38.72	129.78	12383	12912	10196	10373
29.93	179.85	12969	13409	38.91	179.75	12381	12908	10193	10370
29.62	229.79	12976	13420	38.74	229.64	12382	12908	10197	10371
29.81	279.77	12971	13411	38.75	279.79	12373	12906	10194	10367
29.75	329.91	12969	13404	38.74	329.84	12374	12899	10188	10360
11.26	83.93	13209	13462	18.08	83.94	12939	13263	10713	10864
11.43	129.91	13207	13450	18.04	129.43	12940	13263	10713	10866
11.46	179.95	13206	13443	18.07	179.66	12937	13262	10710	10864
11.40	229.78	13205	13440	18.00	229.59	12940	13263	10710	10863
11.56	279.86	13202	13430	18.01	279.70	12934	13262	10708	10861
11.91	329.87	13199	13409	17.98	329.91	12931	13261	10706	10856
-6.95	83.97	13170	14915	-2.52	83.82	13418	13381	10972	11178
-6.48	129.74	13171	14739	-2.66	129.73	13427	13384	10975	11181
-6.49	179.76	13171	14728	-2.51	179.67	13422	13386	10974	11179
-6.38	229.77	13171	14679	-2.38	229.50	13421	13387	10973	11179
-6.38	279.80	13168	14654	-2.67	279.72	13422	13391	10974	11178
-5.88	329.87	13166	14417	-2.81	329.84	13429	13396	10974	11175

AMSU-A1-1 Channels :

Instrument Temp. (C)	Scene Temp. (K)	Ch 6	Ch 7	Ch 9	Ch 10	Ch 11	Ch 12	Ch 13	Ch 14	Ch 15
37.99	83.97	13087	15196	12552	12858	13743	13323	13336	14487	11544
37.66	129.86	13091	15209	12562	12867	13766	13351	13359	14516	11552
38.09	179.79	13077	15202	12542	12859	13748	13322	13342	14488	11540
38.07	229.71	13076	15206	12539	12859	13748	13319	13342	14486	11539
38.10	279.78	13069	15207	12532	12858	13745	13312	13339	14480	11541
38.26	329.83	13058	15206	12518	12853	13732	13293	13328	14461	11537
17.938	83.99	13464	15757	13097	13236	14652	14555	14286	14855	11887
17.947	129.63	13464	15759	13096	13235	14652	14555	14285	14821	11887
18.059	179.71	13462	15757	13094	13234	14650	14547	14279	14748	11887
18.051	229.64	13467	15757	13091	13235	14650	14545	14278	14720	11886
18.081	279.70	13464	15759	13088	13235	14648	14538	14274	14706	11887
18.036	330.06	13460	15772	13085	13238	14653	14533	14275	14634	11890
-2.64	83.88	13650	16213	13464	13413	15217	15627	15003	14080	11946
-2.73	129.72	13656	16217	13469	13414	15226	15633	15011	14087	11949
-2.55	179.70	13654	16214	13462	13412	15225	15624	15008	14086	11950
-2.30	229.51	13655	16213	13460	13414	15224	15610	15004	14088	11958
-2.41	279.73	13658	16218	13460	13418	15232	15615	15010	14092	11963
-2.32	329.94	13663	16222	13459	13427	15239	15619	15012	14096	11978

noises and correspond to an equivalent noise temperature of ~1000K. One can see from Table 3 that the instrument temperature is a dominant factor in determining the magnitude of C_{sint}, which increases as the instrument temperature decreases, but nonlinearly. Only exceptions occur at channels 1 and 14, where the C_{sint} values at -6.6°C and -2.6°C, respectively, are smaller than those at 11.5°C and 18°C. Previous experience [1] shows that such a linear relationship (radiometric counts versus PRT temperatures) would not exist if the instrument temperature is allowed to vary in a range of 4°C during a test cycle.

5. CONCLUSION AND DISCUSSION

We have analyzed the T/V chamber calibration data from the AMSU-A2 PFM and AMSU-A1 FM1, both of which will be flown on NOAA-K. The results show that both models meet the instrument specification in calibration accuracy, nonlinearity, and temperature sensitivity. However, the 3-dB antenna beamwidths (FOVs) at the AMSU-A1 channels exceed the specification limits of 3.3°±10%. Surprisingly, it was found that the calibration accuracies are polarization-dependent. Channels with vertical polarizations show little cold biases at the lowest scene target temperature 84K, while those with horizontal polarizations all have appreciable cold biases, which can be up to 0.6K. The magnitude of these cold biases increases as the difference between the scene target temperature and instrument temperature becomes larger. It is unknown where these polarization-dependent cold biases come from, but it is suspected that some chamber contamination of hot radiance leaked into the areas of cold and scene targets. However, this cannot explain the polarization dependence. Further investigation in this matter is required.

The existence of nonlinearity is shown in most of the channels. We developed a quadratic formula for modeling these nonlinear contributions, which were characterized by a single parameter u. The u values at three instrument temperatures were obtained for individual channels using a least-square fit method. Using the best-fit u values, we performed a series of simulations of the quadratic corrections which would be expected from in-orbit data after the launch of AMSU-A on NOAA-K. In the simulations, the cold space radiance corresponding to the cosmic background temperature 2.73K was adopted as one of the two reference calibration points (the other reference point is at the internal blackbody temperature). The largest nonlinear correction is about 0.3K, which occurs at channel 15 when the instrument temperature is at 38.09° C. Others are less than 0.2K.

In general, the qualities of the T/V chamber test data from both AMSU-A2 PFM and AMSU-A1 FM1 are quite good. Particularly, the instrument temperatures were all stabilized at pre-selected values with total variation less than ±0.5K during each test cycle. This renders the measured instrument nonlinearities more reliable and our analysis results from this study confirm the high quality of the AMSU-A instruments for NOAA-K. However, there are some issues, which should be addressed for improving the calibration results from future instruments so that it may provide us a better understanding of the instrument characteristics. These are detailed below.

The T/V chamber test data from both AMSU-A2 PFM and AMSU-A1 FM1 were taken at three instrument temperatures, of which only one falls in the predicted range of in-orbit operational temperature. The other two instrument temperatures were at 10°C above the maximum and 10°C below the minimum predicted ones. Table 4 lists the predicted range of in-orbit operational instrument temperatures and the actual ones used in the T/V chamber for taking the calibration data. The "nominal" temperature is at the middle of the predicted in-orbit range and the other two, the extreme low (L-10°C) and the extreme high (H+10°C) temperatures, are about 20°C below and above the nominal one, respectively. From the instrument's point of view, it is prudent to calibrate the instruments at an extreme low and extreme high instrument temperatures so that a large safety margin of instrument performance can be established. However, from a scientific point of view, it would be better that the calibration is done with three instrument temperatures which are all within the range of predicted in-orbit operational temperatures. An increment of 20°C steps in instrument temperature is too large for adequately characterizing a new instrument, particularly high accuracy in extracting the nonlinearity parameters is required. We showed in this study that the effects of

Table 4. AMSU-A Instrument Temperatures (°C) of predicted in-orbit range and the actual values used in T/V chamber tests.

Predicted or T/V	AMSU-A2 Instrument Temperatures.(°C)					AMSU-A1-1/A1-2 Instrument Temperature.(°C)					Remarks
	L-10°C	L	N	H	H+10°C	L-10°C	L	N	H	H+10°C	
Predicted		3	12	20			8	18	28		In-Orbit
T/V Tests	-6.6		11.5		29.7	-2.6		18		38	Pre-Launch Calibration

Note: L = Low, N = Nominal, H = High

instrument temperature on the warm load correction factor, nonlinearity corrections, and radiometric counts at zero radiance are all nonlinear. For an arbitrary instrument temperature, the first two parameter values (which will be used in processing the in-orbit data) must be interpolated from the quantities at the three selected temperatures used for pre-launch calibration. The interpolation error would be minimized if all three instrument temperatures (used in T/V chamber test data) are within the predicted in-orbit range. Furthermore, additional calibrations at the low and high instrument temperature (see Table 4) of the predicted range in space would provide us a way to check the peculiar patterns of the nonlinearity corrections (Figure 4) and warm load correction factors (Figure A-1). The original AMSU-A test plan [4,5] also specifies that the calibrations be done at the low, nominal, and high instrument temperatures of predicted range in space. To satisfy both the instrumental and scientific goals, calibration should be performed at all five instrument temperatures as listed in Table 4. For purpose of reducing cost, calibrations at the extreme low and extreme high instrument temperatures may be done with less than six scene temperatures, since it only needs to demonstrate that the AMSU-A instruments will still perform within specification in such cases. However, calibrations at the other three instrument temperatures (i.e., predicted low, nominal, and high) should be performed at all six scene temperatures since these data will be used to characterize the instruments.

The warm load correction factors (as shown in Figure A-1) will be used for processing AMSU-A data from every scan line. One would like to make sure that the "measured" values are accurate. None of the warm-load-correction patterns (Figure A-1) looks alike to each other. Perhaps, more than one measurement of such data should be taken to show that the patterns of instrument-temperature dependence of these correction factors can be repeated. It would be desirable to calculate these factors from data taken at both the beginning and end of the calibration process.

The polarization dependence of the calibration accuracy, which produces large cold biases at all channels with horizontal polarization, is an interesting but peculiar phenomena of the calibration data. If the origin of this contamination comes from the T/V chamber, perhaps no correction is necessary for processing the in-orbit data. However, if it originates within the instrument system, then correction is needed because the cold bias will also appear in space (after launch.) A bias of 0.5K should not be ignored in the latter case. It would be a giant step forward in improving the calibration accuracy if the source of contamination could be found and eliminated.

ACKNOWLEDGEMENTS: The computations and processing of the calibration data were done on the VAX Computer at the Oceanic Sciences Branch, SRL. I am indebted to Richard Legeckis and Pablo Clemente-Colon for their expert help in using the computer. I would like to thank David Wark for his continued support and his valuable advice in resolving many of the technical problems related to anomalies and waivers encountered in the AMSU-A Project. Thanks go to J. Philip Green of NOAA/SPO and Sergey Krimchansky of NASA/GSFC for their management of the AMSU-A Program. John Alishouse made helpful comments on the manuscript. Tina Cashman, who edited the first draft, is gratefully acknowledged. Aerojet is the primary AMSU-A contractor for building the instruments and performed the initial calibration analysis to demonstrate the fine quality of the instrument.

REFERENCES

[1]. "AMSU-A Engineering Model Calibration," NOAA Technical Report NESDIS 68, 1993, Tsan Mo, Michael Weinreb, Norman Grody, and David Wark.

[2]. "NOAA-KLM Data Processing Specifications," NOAA/NESDIS Internal Memorandum, D. Wark et. al, 1994.

[3]. "Calibration Log Book for AMSU-A2," Report #10401, 1994, Aerojet, Azusa, CA 91702. "Calibration Log Book for AMSU-A1," Report #10481, 1994, Aerojet, Azusa, CA 91702.

[4]. "Performance and Operation Specification for the AMSU-A," Contract Attachment B, S-480-13, NASA/GSFC, August 1984.

[5]. "System Calibration Test Procedure for the AMSU-A1 System," AE-26156/5, February 1992, Aerojet, Azusa, CA 91702.

[6]. PRT Handbook, Bulletin 1042, 1986, Rosemount Inc., Burnsville, MN 55337.

[7]. "The Advanced Microwave Sounding Unit-A," P. K. Patel and J. Mentall, in *Microwave Instrumentation for Remote Sensing of the Earth,* SPIE Vol. 135, pp.130-135; Orlando, April 13-14, 1993.

APPENDIX A

A.1 *Warm Load Correction*

The in-flight warm load correction was calculated according to a formula developed by Aerojet [3]. For each AMSU-A antenna system, a special set of calibration data were acquired by setting the temperature of its variable scene target equal to that of the internal blackbody (warm) target. The physical temperature T_w of the internal blackbody target was determined from the PRT counts as described in Section 2. The radiometric temperature T_{wrad} of the blackbody (in-flight warm load) was calculated (for each scan in the data set) by the formula

$$T_{wrad} = T_{sprt} + (T_{sprt} - T_c)\left(\frac{C_w - C_s}{C_s - C_c}\right) \qquad \text{(A-1)}$$

where: T_{sprt} = PRT temperature of the variable scene target,

T_c = PRT temperature of the cold target,

C_w = the average of two radiometric counts from the warm target,

C_c = the average of two radiometric counts from the cold target, and

C_s = radiometric counts from the variable scene target.

One should note that temperatures, T_{sprt} and T_c, from the scene and cold targets are used as the two reference calibration points in Equation (A-1) and the radiometric temperature for the warm target is calculated.

The in-flight warm load correction factor ΔT_w was computed from the formula

$$\Delta T_w = \frac{1}{N}\sum_{i=1}^{N}(T_{wrad} - T_w)_i \qquad \text{(A-2)}$$

where N(=725) represents the number of scans in the data set. The ΔT_w values at three instrument (RF Shelf) temperatures for each AMSU-A antenna system are listed in Table A-1. For AMSU-A1, the ΔT_w values for both PLLO#1 and PPLO#2 were calculated.

Figure A-1 shows the calculated ΔT_w values versus the channels. Noticeable features in Figure A-1 are briefly described below.

The ΔT_w values for AMSU-A2 PFM are all negative and vary approximately linearly with the instrument temperatures. The negative ΔT_w values imply that the radiometric temperatures are smaller than its physical temperature. This is unusual, particularly because it occurs at all three instrument temperatures.

The ΔT_w values for channels in AMSU-A1-2, FM1 are independent of instrument temperature. In contrast, the calculated ΔT_w values at the AMSU-A1-1 channels show strong instrument-temperature dependence. The ΔT_w values at the nominal instrument temperature 18.03° C are approximately three times larger than the ones at the other two instrument temperatures, except in the case of channel 9. These warm load correction factors form a triangle-pattern dependence upon instrument temperature. It is difficult to understand such behavior of the ΔT_w values. Actually, only the ΔT_w values at channel 9 are considered reasonable and show the effect of instrument temperature on the correction factor that would be expected from a linear (near linear) system. Furthermore, the pattern of the ΔT_w values from the PLLO#2 case is completely different, as shown in the bottom part of Figure A-1, where the triangle-shaped instrument-temperature dependence disappears.

Figure A-2 shows the results of calculated calibration accuracy, if the individual ΔT_w values from AMSU-A1-1 channels (PLLO#1) in Figure A-1 were used. One can see that all ΔR values at the nominal instrument temperature 18.03° C near the warm load radiance, R_w, are negative, instead of being zero. This shows that these measured values of warm load correction (at the instrument temperature 18.03° C) are all too large and that overcorrections are resulted in the calculations.

Based on the above results, we decided that the individual ΔT_w values of AMSU-A1-1 channels (PLLO#1) in Figure A-1 should not be used in our calibration. Instead, the mean values (Table A-1) of the three sets of ΔT_w values from three instrument temperatures were used in this study. The results in Figure 1 were obtained with the mean ΔT_w values from AMSU-A1-1 channels.

A.2 *Channel Characteristics, Specification, and Measurement Errors*

Table A-2 lists the AMSU-A channel characteristics and specifications [4]. Included also are the measured channel frequencies, 3-dB bandwidths, NEΔT, and FOV (antenna beamwidths). One should note that the FOVs at most of the AMSU-A1 channels exceed the specification limits of 3.3°±10%. The bias and random errors [3] in measurements from individual AMSU-A systems are listed in Table A-3.

Table A-1. Warm load corrections (K) at three instrument temperatures.

AMSU-A2 Channels: AMSU-A1-2 Channels:

Instrument Temperature (C)	CH. 1	CH. 2	Instrument Temperature (C)	CH. 3	CH. 4	CH. 5	CH. 8
29.63	-0.007	-0.133	38.78	0.097	0.009	0.013	-0.009
11.61	-0.046	-0.230	17.98	0.112	0.022	0.011	0.005
-6.42	-0.127	-0.392	-2.61	0.117	0.006	-0.002	-0.007
Mean	-0.060	-0.252		0.109	0.012	0.007	-0.004

AMSU-A1-1 Channels (PLLO #1)

Instrument Temperature (C)	CH. 6	CH. 7	CH. 9	CH. 10	CH. 11	CH. 12	CH. 13	CH. 14	CH. 15
38.09	0.069	0.008	0.134	0.061	0.058	0.046	0.074	0.038	0.067
18.03	0.193	0.127	0.092	0.165	0.164	0.169	0.169	0.141	0.188
-2.41	0.012	0.006	-0.089	0.032	0.033	0.041	0.063	-0.020	0.007
Mean	0.091	0.047	0.046	0.086	0.085	0.085	0.102	0.053	0.087

AMSU-A1-1 Channels (PLLO #2)

Instrument Temperature (C)	CH. 9	CH. 10	CH. 11	CH. 12	CH. 13	CH. 14
38.78	0.096	0.078	0.076	0.086	0.076	0.051
16.43	-0.071	0.080	0.072	0.013	0.076	0.020
-2.22	-0.022	0.059	0.083	0.048	0.040	0.001
Mean	0.001	0.072	0.077	0.049	0.064	0.024

Table A-2. Channel characteristics and specifications of AMSU-A2 PFM and AMSU-A1 FM1 for NOAA-K.

Channel Number	Channel Frequency (MHz)		No. of Bands	Measured 3-dB Bandwidth (MHz)	NEΔT (K)		Beam # Efficiency	Polarization (NADIR)	FOV** (deg.)	Remarks
	Specification	Measured *			Spec.	Measred				
1	23800	23800.37	1	251.02	0.30	0.211	95%	V	3.52	A2/PFM
2	31400	31400.42	1	161.20	0.30	0.265	97%	V	3.40	"
3	50300	50299.91	1	161.14	0.40	0.219	95%	V	3.75	A1/FM1
4	52800	52799.39	1	380.52	0.25	0.143	95%	V	3.72	"
5	53596 ± 115	53595.41 ± 115	2	168.20 I 168.20	0.25	0.148	95%	H	3.69	"
6	54400	54399.53	1	380.54	0.25	0.154	95%	H	3.68	"
7	54940	54940.64	1	380.56	0.25	0.132	95%	V	3.61	"
8	55500	55498.70	1	310.34	0.25	0.141	96%	H	3.62	"
9	fo = 57290.344	fo = 57290.33	1	310.42	0.25	0.236	96%	H	3.51	"
10	fo ± 217	fo ± 217	2	76.58 I 76.58	0.40	0.250		H	"	"
11	fo ± 322.2 ± 48	fo ± 322.2 ± 48	4	34.28 / 35.11 I 35.11 / 34.28	0.40	0.280		H	"	"
12	fo ± 322.2 ± 22	fo ± 322.2 ± 22	4	15.08 / 15.29 I 15.29 / 15.08	0.60	0.400		H	"	"
13	fo ± 322.2 ± 10	fo ± 322.2 ± 10	4	7.92 / 7.93 I 7.93 / 7.92	0.80	0.539		H	"	"
14	fo ± 322.2 ± 4.5	fo ± 322.2 ± 4.5	4	2.94 / 2.92 I 2.92 / 2.94	1.20	0.914		H	"	"
15	89000	88997.00	1	1998.98	0.50	0.166	98%	V	3.80	"

* At temperature 18 degree C. ** Note : Specification requires 3.3 degrees ± 10% for all channels. # Measured.

Table A-3. Uncertainty in brightness temperatures and measurement errors.

Origin of Errors	AMSU-A2 (Ch . 1 and 2)		AMSU-A1 (Ch. 3 - 15)	
	Bias (K)	Random (K)	Bias (K)	Random (K)
Warm Target	-0.050	±0.122	-0.050	±0.122
Cold Target	0.024	±0.105	0.024	±0.091
Scene Target	0.002	±0.101	0.002	±0.090

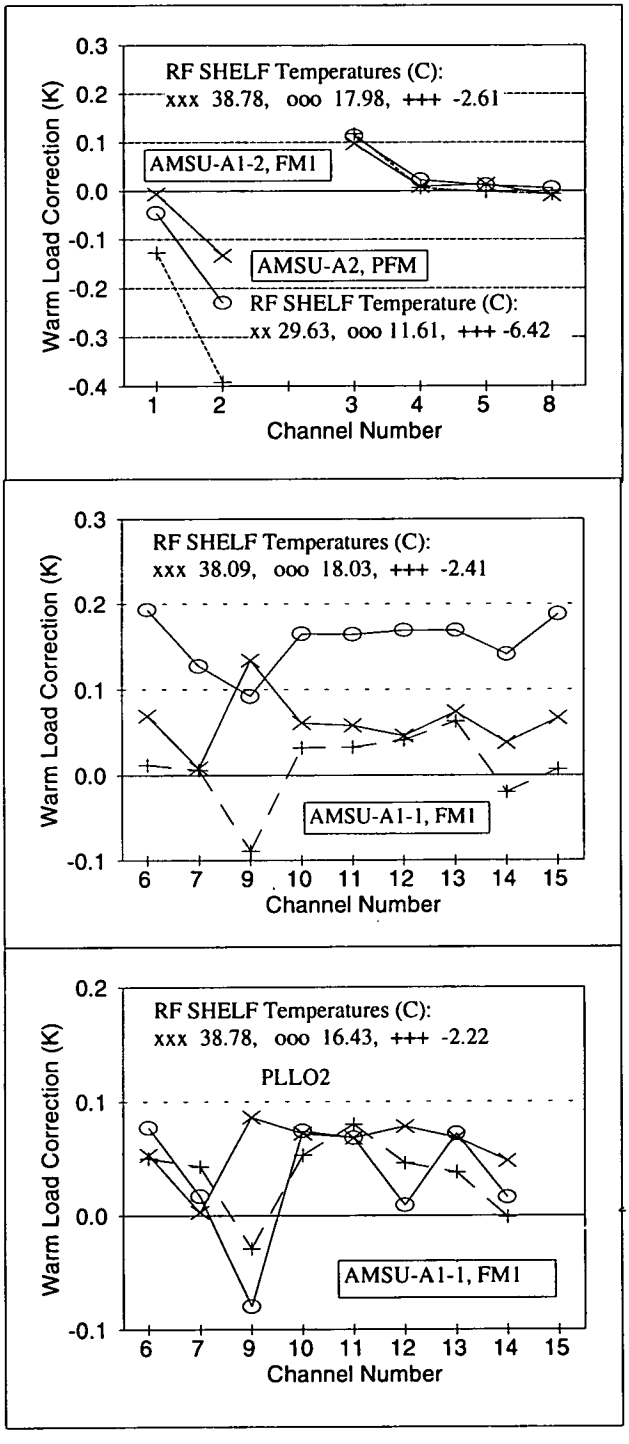

Fig. A-1. Warm load correction factors calculated for each AMSU-A antenna system at three instrument temperatures. The bottom one was obtained with the backup PLLO#2 in channels 9-14.

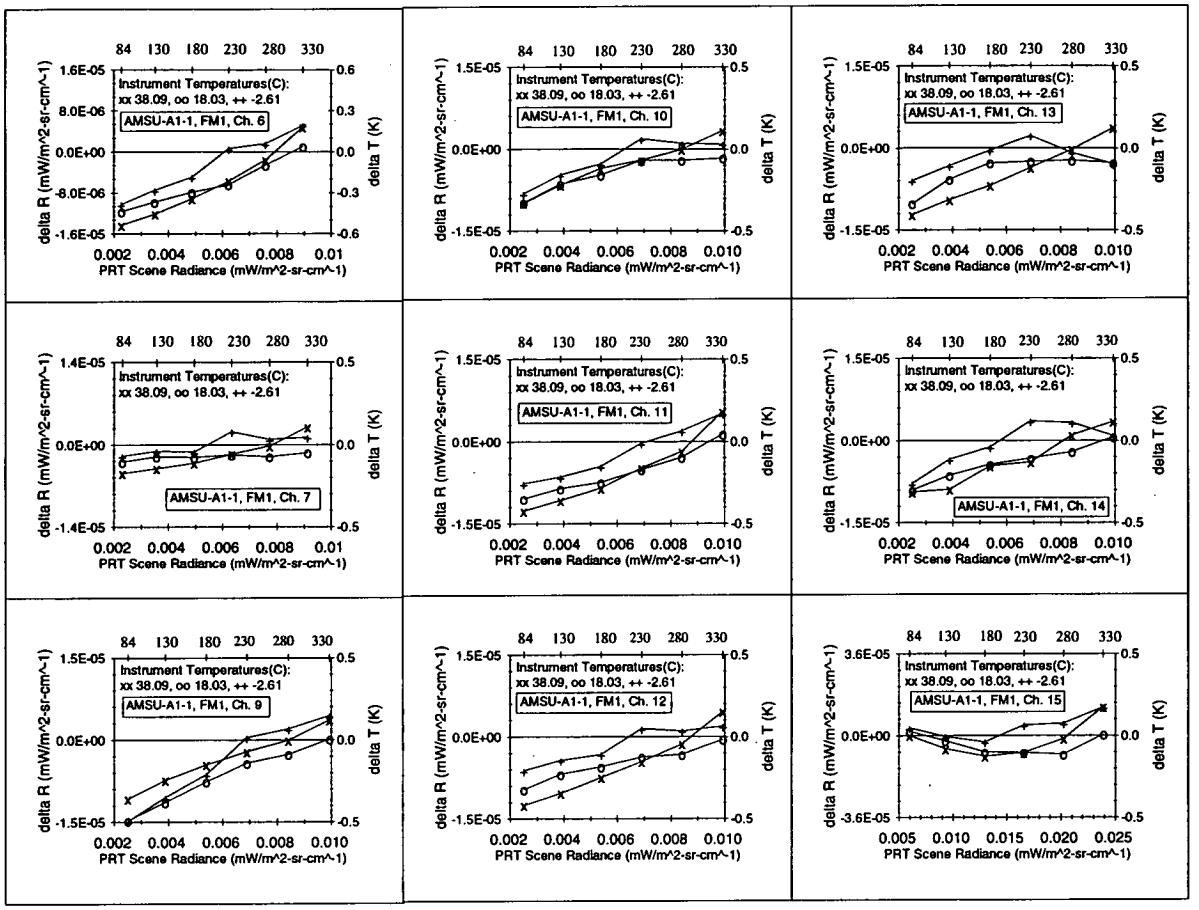

Fig. A-2. Calibration accuracy: delta R versus PRT scene radiances for AMSU-A1-1 channels. The warm load correction factors in Figure A-1 were used in these calculations. Note that the delta R values are all negative at the nominal instrument temperature 18.03 C. One should compare these plots to those in Figure 1.

APPENDIX B

COEFFICIENTS FOR AMSU-A2 PFM AND AMSU-A1 FM1

B.1 *Polynomial Coefficients for Converting PRT Counts into Temperatures*

The two-step process for deriving the PRT temperatures from PRT counts C_k is briefly described here. First the C_k from PRT k is converted into resistance r_t (in ohms) by a polynomial

$$r_t = \sum_{i=0}^{3} A_i C_k^i \qquad \text{(B-1)}$$

where the coefficients A_i for individual PRTs and temperature sensors were provided by Aerojet. Once the resistance r_t is known, then one can calculate the PRT temperature t (in Celsius) from the Callendar-Van Dusen equation [6], which is given by

$$\frac{r_t}{r_o} = 1 + \alpha\left[t - \delta\left(\frac{t}{100} - 1\right)\left(\frac{t}{100}\right) - \beta\left(\frac{t}{100} - 1\right)\left(\frac{t}{100}\right)^3\right] \qquad \text{(B-2)}$$

where: r_t = resistance (in ohms) at temperature t (°C) of the blackbody target

r_o = resistance at t = 0°C (supplied by the manufacturer via Aerojet)

β = 0 for t > 0°C, and 0.11 for t < 0°

α and δ are constants provided by the manufacturer via Aerojet.

Calculation shows that the error is negligible by setting $\beta = 0$ in Equation (B-2). In such case, one can solve the quadratic equation for t in terms of r_t. Then the PRT temperature in degree Kelvin is obtained from t + 273.15. By this way, data sets of PRT temperatures versus counts for individual PRTs are computed. Then Equation (1) is applied to fit these data sets for obtaining the polynomial coefficients f_{kj} for individual PRTs and housekeeping sensors. These best-fit coefficients are listed in Tables B-1 and B-2, respectively, for AMSU-A1 and AMSU-A2. Test calculations show that these polynomials are highly accurate in reproducing temperatures of PRTs and sensors.

Table B-1. AMSU-A1 FM1 : Polynomial coefficients for converting PRT counts into temperatures, as defined in Equation (1).

PRT Number	Description	fk0 (K)	fk1 (K/count)	fk2 (K/count^2)	fk3 (K/count^3)
1	Scan Motor A1-1	263.0037	1.747464E-03	3.611793E-09	1.408073E-14
2	Scan Motor A1-2	263.0755	1.737651E-03	4.401445E-09	1.651136E-15
3	Feedhorn A1-1	262.9443	1.747953E-03	3.692945E-09	1.236913E-14
4	Feedhorn A1-2	263.0390	1.739450E-03	4.221214E-09	3.747511E-15
5	RF Mux A1-1	263.0722	1.747151E-03	3.735050E-09	1.132005E-14
6	RF Mux A1-2	262.9747	1.737891E-03	4.241792E-09	3.482516E-15
7	L.O. CH 3	263.0540	1.748261E-03	3.730504E-09	1.180654E-14
8	L.O. CH 4	262.9409	1.736642E-03	4.349951E-09	1.296027E-15
9	L.O. CH 5	263.0854	1.735083E-03	4.282954E-09	3.003631E-15
10	L.O. CH 6	262.8903	1.750977E-03	3.637912E-09	1.331306E-14
11	L.O. CH 7	263.0363	1.747121E-03	3.651951E-09	1.337592E-14
12	L.O. CH 8	263.0474	1.734271E-03	4.391040E-09	1.000835E-15
13	PLLO #1 CH 9-14	263.2229	1.751721E-03	3.622826E-09	1.276853E-14
14	PLLO #2 CH 9-14	262.9726	1.736947E-03	4.313505E-09	2.238924E-15
15	PLLO (Ref. Osc.)	263.0713	1.748204E-03	3.651635E-09	1.366764E-14
16	L.O. CH 15	263.0214	1.737994E-03	4.272213E-09	3.144219E-15
17	Mixer/IF CH 3	263.1502	1.751596E-03	3.733117E-09	1.213597E-14
18	Mixer/IF CH 4	262.9138	1.737586E-03	4.273391E-09	3.773862E-15
19	Mixer/IF CH 5	262.9436	1.746811E-03	3.715164E-09	1.220530E-14
20	Mixer/IF CH 6	263.1028	1.740953E-03	4.301377E-09	2.778946E-15
21	Mixer/IF CH 7	263.0626	1.751180E-03	3.709273E-09	1.264067E-14
22	Mixer/IF CH 8	262.9497	1.739036E-03	4.289452E-09	3.000804E-15
23	Mixer/IF CH 9/14	263.0612	1.748672E-03	3.651322E-09	1.348387E-14
24	Mixer/IF CH 15	263.0224	1.734811E-03	4.284050E-09	3.032046E-15
25	IF Amp. Ch.11/14	263.5755	1.749622E-03	3.732910E-09	1.228633E-14
26	IF Amp. Ch. 9	263.2024	1.739840E-03	4.245337E-09	3.929503E-15
27	IF Amp. Ch. 10	262.9374	1.750283E-03	3.678020E-09	1.279883E-14
28	IF Amp. Ch. 11	262.9866	1.739247E-03	4.256647E-09	3.939451E-15
29	IF Amp. Ch. 12	263.0103	1.746012E-03	3.718877E-09	1.227157E-14
30	IF Amp. Ch. 13	262.9475	1.738816E-03	4.322414E-09	2.640587E-15
31	IF Amp. Ch. 14	262.9747	1.750096E-03	3.720513E-09	1.176121E-14
32	DC/DC Converter	263.0440	1.736559E-03	4.289366E-09	3.027244E-15
33	RF Shelf A1-1	263.4052	1.681521E-03	3.948928E-09	1.345825E-14
34	RF Shelf A1-2	263.0074	1.737507E-03	4.300952E-09	2.651179E-15
35	Detector/Pre-Amp	263.0804	1.776352E-03	4.423964E-09	3.883034E-15
36*	A1-1 Warm Load #1	254.1019	1.688278E-03	6.244238E-09	3.328028E-14
37	A1-1 Warm Load #2	254.2900	1.686999E-03	6.357508E-09	3.146837E-14
38	A1-1 Warm Load #3	254.0750	1.685169E-03	6.328462E-09	3.163947E-14
39	A1-1 Warm Load #4	253.9840	1.684983E-03	6.380120E-09	3.072460E-14
40	A1-1 Wm Ld Center	254.1018	1.680988E-03	6.573108E-09	2.706750E-14
41	A1-2 Warm Load #1	254.2721	1.685880E-03	6.320013E-09	3.160865E-14
42	A1-2 Warm Load #2	253.9749	1.685104E-03	6.402781E-09	3.019014E-14
43	A1-2 Warm Load #3	254.0395	1.686245E-03	6.167368E-09	3.503316E-14
44	A1-2 Warm Load #4	254.1039	1.684664E-03	6.251739E-09	3.330978E-14
45	A1-2 Wm Ld Center	254.1421	1.685286E-03	6.308630E-09	3.144644E-14

*** PRT of AMSU-A1-1 Warm Load #1 is bad**

Table B-2. AMSU-A2 PFM: Polynomial coefficients for converting PRT counts into temperatures, as defined in Equation (1).

PRT Number	Description	fk0 (K)	fk1 (K/count)	fk2 (K/count^2)	fk3 (K/count^3)
1	Scan Motor	262.8483	1.744870E-03	3.656985E-09	1.311605E-14
2	Feedhorn	262.8909	1.745131E-03	3.618670E-09	1.371539E-14
3	RF Mux	262.8583	1.738158E-03	4.182846E-09	4.551534E-15
4	Mixer/IF CH	262.9412	1.745020E-03	3.638992E-09	1.317258E-14
5	Mixer/IF CH 2	263.0224	1.738089E-03	4.475776E-09	-2.782349E-16
6	L.O. CH 1	262.8308	1.745703E-03	3.652799E-09	1.288072E-14
7	L.O. CH 2	262.8446	1.733296E-03	4.214177E-09	3.241416E-15
8	Comp. Motor	262.7900	1.734460E-03	4.373190E-09	1.175410E-15
9	Sub Reflector	262.7894	1.746871E-03	3.604260E-09	1.427609E-14
10	DC/DC Conver	262.9737	1.734227E-03	4.156827E-09	4.614430E-15
11	RF Shelf	262.8805	1.746935E-03	3.662064E-09	1.326031E-14
12	Dect. Pre-Amp	262.8441	1.736258E-03	4.159231E-09	5.129305E-15
13	Warm Load Center	253.9989	1.638866E-03	6.007023E-09	2.812463E-14
14	Warm Load #1	254.0397	1.636785E-03	6.027363E-09	2.824335E-14
15	Warm Load #2	253.9349	1.642202E-03	5.981135E-09	2.918848E-14
16	Warm Load #3	254.0187	1.638825E-03	6.018147E-09	2.859953E-14
17	Warm Load #4	253.9916	1.638811E-03	6.048192E-09	2.740716E-14
18	Warm Load #5	253.9744	1.638622E-03	6.003124E-09	2.799640E-14
19	Warm Load #6	253.9943	1.637949E-03	6.066317E-09	2.668021E-14

B.2 *Correction to In-orbit Cold Space Calibration*

For in-orbit cold space calibration, there is an uncertainty due to antenna side lobe interference with the Earth limb and spacecraft. The contribution from this uncertainty should be added to the cold space cosmic background temperature of 2.73K. Therefore, the "corrected" cold space temperature T_{cc} can be represented by

$$T_{cc} = 2.73 + \Delta T_c \tag{B-3}$$

where ΔT_c represents the contribution due to antenna side lobe interference with the Earth limb and spacecraft. Aerojet made estimates of ΔT_c for individual channels and its values [3] are listed in Table B-3. These ΔT_c values will be used initially and the final optimal values for ΔT_c will be determined from the post-launch calibration.

Table B-3. Values of ΔT_c and limits of blackbody count variations.

Channel	ΔT_c (K)	ΔC_w (count)
1	0.74	12
2	0.44	12
3	1.19	12
4	1.22	12
5	1.28	12
6	1.49	12
7	1.33	12
8	1.25	12
9	1.43	12
10	1.43	12
11	1.43	16
12	1.43	16
13	1.43	20
14	1.43	40
15	0.91	15

B.3 *Limit of Blackbody Counts Variation*

For each scan, the blackbody count C_w is the average of two samples. If the two samples of the blackbody differ by more than a pre-set limit of blackbody count variation ΔC_w, the data in the scan will not be used. The ΔC_w values for individual channels are listed in Table B-3. These ΔC_w values, which equal approximately 3σ (where σ is the standard deviation of the internal blackbody counts), are calculated from the T/V calibration data.

B.4 *Pre-launch Determined Weight Factors w_k for the Internal Blackbody PRTs*

The weight factors w_k (see Equation 2) assigned to individual PRTs in the internal blackbody targets are listed in Table B-4. As discussed in Section 2, the PRT #1 in AMSU-A1-1 FM1 is bad and therefore the $w_1 = 0$ is assigned to it. All other PRTs are good.

Table B-4. Pre-launch determined weight factors w_i assigned to individual PRTs in blackbody targets.

Antenna System	w_1	w_2	w_3	w_4	w_5	w_6	w_7
AMSU-A2	1	1	1	1	1	1	1
AMSU-A1-1	0	1	1	1	1		
AMSU-A1-2	1	1	1	1	1		

B.5 *Conversion Coefficients of Analog Data*

AMSU-A instrument has an analog telemetry bus to monitor key temperatures and voltages through the spacecraft. The resolutions of the analog telemetry received on the ground is 20 mV for one part in 256. To convert the analog data into physical quantities y, one must multiply the analog values by 0. 02V (20mV) to obtain the measured output, x, in volts and then uses the conversion equation

$$y = B + Mx \tag{B-4}$$

where the values of B and M are given in Tables B-5 and B-6 for AMSU-A2 and -A1, respectively.

Table B-5. AMSU-A2 PFM: Analog data conversion coefficients.

UIIS Ref #	Description	Units (of y)	M	B
1	RF Shelf Temperature	K	68.027	0
2	Compensator Motor Temperature	K	68.027	0
3	Scan Motor Temperature	K	68.027	0
4	Warm Load Tempterature	K	68.027	0
5	Antenna Drive Motor Current (average)	mA	27.300	0
6	Compensator Motor Current (average)	mA	27.300	0
7	Signal Processing +15Vdc	V	5.017	0
8	Antenna Drive +15Vdc	V	4.941	0
9	Signal Processing -15Vdc	V	-2.030	-9.000
10	Antenna Drive -15Vdc	V	-1.958	-9.000
11	Receiver +8Vdc	V	1.843	0
12	Radiometer, receiver, processor +Vdc	V	1.680	0
13	Antenna Drive +5Vdc	V	1.635	0
14	Gunn Diode Osc. #1 (hannel 1)	V	2.011	0
15	Gunn Diode Osc. #2 (hannel 2)	V	1.675	0

Table B-6. AMSU-A1 FM1: Analog data conversion coefficients.

UIIS Ref #	Description	Units (of y)	M	B
1	A1-1 Scan Motor Temperature	K	68.027	0
2	A1-2 Scan Motor Temperature	K	68.027	0
3	A1-1 RF Shelf Temperature	K	68.027	0
4	A1-2 RF Shelf Temperature	K	68.027	0
5	A1-1 Warm Load Temperature	K	68.027	0
6	A1-2 Warm Load Temperature	K	68.027	0
7	A1-1 Antenna Drive Motor Current (average)	mA	20.000	0
8	A1-2 Antenna Drive Motor Current (average)	mA	20.000	0
9	Signal Processing +15Vdc	V	5.000	0
10	Antenna Drive +15Vdc	V	5.000	0
11	Signal Processing -15Vdc	V	-2.000	-9.0
12	Antenna Drive -15Vdc	V	-2.000	-9.0
13	Receiver +8Vdc	V	1.840	0
14	Radiometer, receiver, processor +Vdc	V	1.700	0
15	Antenna Drive +5Vdc	V	1.680	0
16	Phase Locked Loop (Ch. 9/14) +8.5VDC	V	2.010	0
17	Phase Locked Loop (Ch. 9/14) +15VDC	V	5.030	0
18	Phase Locked Loop (Ch. 9/14) -15VDC	V	-1.940	-9.0
19	Gunn Diode Osc. #4 (hannel 3)	V	1.800	0
20	Gunn Diode Osc. #5 (hannel 4)	V	1.790	0
21	Gunn Diode Osc. #6 (hannel 5)	V	1.790	0
22	Gunn Diode Osc. #3 (hannel 6)	V	1.780	0
23	Gunn Diode Osc. #2 (hannel 7)	V	1.780	0
24	Gunn Diode Osc. #1 (hannel 8)	V	1.790	0
25	PLLO#1 Lock Detect	V	7.400	-14.8
26	PLLO#2 Lock Detect	V	7.400	-14.8
27	Gunn Diode Osc. #7 (hannel 15)	V	1.650	0

APPENDIX C

NOAA POLAR ORBITER LEVEL 1B DATA

The NOAA Polar Orbiter Level 1b data are raw data that have been quality controlled and assembled into discrete data sets, to which Earth location and calibration information are appended but not applied. For each channel, one can convert Equation (4) into the form,

$$R_s = a_0 + a_1 C_s + a_2 C_s^2 \qquad \text{(C-1)}$$

where the calibration coefficients a_i (where i = 0, 1, and 2) can be expressed in terms of R_w, G, $\overline{C_w}$, and $\overline{C_c}$. This can be accomplished by rewriting the right-hand side of Equation (4) in powers of C_s and equates the a_i's to the coefficients of the same powers of C_s. The results are,

$$a_0 = R_w - \frac{\overline{C_w}}{G} + u\frac{\overline{C_w}\,\overline{C_c}}{G^2} \qquad \text{(C-2)}$$

$$a_1 = \frac{1}{G} - u\frac{\overline{C_w} + \overline{C_c}}{G^2} \qquad \text{(C-3)}$$

and

$$a_2 = \frac{u}{G^2} \qquad \text{(C-4)}$$

These calibration coefficients will be calculated for each scan at each channel and appended to the 1B data. With these coefficients, one can simply apply Equation (C-1) to obtain the scene radiance R_s. Users, who prefer brightness temperature instead of radiance, can make the simple conversion,

$$T_s = B^{-1}(R_s) \qquad \text{(C-5)}$$

where $B^{-1}(R_s)$ is the inverse of the Planck function for a radiance R_s. The T_s is the converted brightness temperature (or radiometric temperature).

One should note that the coefficients a_0, a_1, and a_2 are functions of the instrument temperature. Therefore, they are not constant in general and should be re-calculated at each scan.

(Cont'd from front inside cover)

NESDIS 49 Implementation of Reflectance Models in Operational AVHRR Radiation Budget Processing. V. Ray Taylor, February 1990.

NESDIS 50 A Comparison of ERBE and AVHRR Longwave Flux Estimates. A. Gruber, R. Ellingson, P. Ardanuy, M. Weiss, S. K. Yang, (Contributor: S.N. Oh).

NESDIS 51 The Impact of NOAA Satellite Soundings on the Numerical Analysis and Forecast System of the People's Republic of China. A. Gruber and W. Zonghao, May 1990.

NESDIS 52 Baseline Upper Air Network (BUAN) Final Report. A. L. Reale, H. E. Fleming, D. Q. Wark, C. S. Novak, F. S. Zbar, J. R. Neilon, M. E. Gelman and H. J. Bloom, October 1990.

NESDIS 53 NOAA-9 Solar Backscatter Ultraviolet (SBUV/2) Instrument and Derived Ozone Data: A Status Report Based on a Review on January 29, 1990. Walter G. Planet, June 1990.

NESDIS 54 Evaluation of Data Reduction and Compositing of the NOAA Global Vegetation Index Product: A Case Study. K. P. Gallo and J. F. Brown, July 1990.

NESDIS 55 Report of the Workshop on Radiometric Calibration of Satellite Sensors of Reflected Solar Radiation, March 27-28, 1990, Camp Springs, MD. Peter Abel (Editor), July 1990.

NESDIS 56 A Noise Level Analysis of Special 10-Spin-Per-Channel VAS Data. Donald W. Hillger, James F. W. Purdom and Debra A. Lubich, February 1991.

NESDIS 57 Water Vapor Imagery Interpretation and Applictions to Weather Analyis and Forecasting. Roger B. Weldon and Susan J. Holmes, April 1991.

NESDIS 58 Evaluating the Design of Satellite Scanning Radiometers for Earth Radiation Budget Measurements with System, Simulations. Part 1: Instantaneous Estimates. Larry Stowe, Philip Ardanuy, Richard Hucek, Peter Abel and Herbert Jacobowitz, October 1991.

NESDIS 59 Interactive Digital Image Display and Analysis System (IDIDAS) User's Guide. Peter J. Celone and William Y. Tseng, October 1991.

NESDIS 60 International Dobson Data Workshop Summary Report. Robert D. Hudson (University of Maryland) and Walter G. Planet, February 1992.

NESDIS 61 Tropical Cyclogenesis in the Western North Pacific. Raymond M. Zehr, July 1992.

NESDIS 62 NOAA Workshop on Climate Scale Operational Precipitation and Water Vapor Products. Ralph Ferraro (Editor), October 1992.

NESDIS 63 A Systematic Satellite Approach for Estimating Central Pressures of Mid-Latitude Oceanic Storms. Frank J. Smigielski and H. Michael Mogil, December 1992.

NESDIS 64 Adjustment of TIROS Operational Vertical Sounder Data to a Vertical View. David Q. Wark, March 1993.

NESDIS 65 A Noise Level Analysis of Special Multiple-Spin VAS Data During Storm-fest. Donald W. Hillger, James F.W. Purdom and Debra A. Molenar, April 1993.

NESDIS 66 Catalogue of Heavy Rainfall Cases of Six Inches or more over the Continental U.S. during 1992. Charles Kadin, April 1993.

NESDIS 67 The Relationship between Water Vapor Plumes and Extreme Rainfall Events during the Summer Season. Wassila Thiao, Roderick A. Scofield and Jacob Robinson, May 1993.

NESDIS 68 AMSU-A Engineering Model Calibration. Tsan Mo, Michael P. Weinreb, Norman C. Grody and David Q. Wark, June 1993.

NESDIS 69 Nonlinearity Corrections for the Thermal Infrared Channels of the Advanced Very High Resolution Radiometer: Assessment and Recommendations. C.R. Nagaraja Rao (Editor), June 1993.

NESDIS 70 Degradation of the Visible and Near-Infrared Channels of the Advanced Very High Resolution Radiometer on the NOAA-9 Spacecraft: Assessment and Recommendations for Corrections. C.R. Nagaraja Rao (Editor), June 1993.

NESDIS 71 Spectral Radiance-Temperature Conversions for Measurements by AVHRR Thermal Channels 3,4,5. Paul A. Davis, August 1993.

NESDIS 72 Summary of the NOAA/NESDIS Workshop on Development of a Global Satellite/in Situ Environmental Database. Edited by K.P. Gallo and D.A. Hastings, August 1993.

NESDIS 73 Intercomparison of the Operational Calibration of GOES-7 and METEOSAT-3/4. W. Paul Menzel, Johannes Schmetz, Steve Nieman, Leo Van de Berg, Volker Gaertner, and Timothy J. Schmit, September 1993.

NESDIS 74 Dobson Data Re-Evaluation Handbook. Robert D. Hudson and Walter G. Planet (Eds), October 1993.

NESDIS 75 Detection and Analysis of Fog at Night Using GOES Multispectral. Gary P. Ellrod, February 1994.

NESDIS 76 Tovs Operationa Sounding Updgrades: 1990-1992. A. Reale, M. Chalfant, R. Wagoner, T. Gardner and L. Casey, March 1994.

NESDIS 77 NOAA Polar Satellite Calibration: A System Description. Cecil A. Paris, April 1994.

NESDIS 78 Post-Launch Calibration of the Visible and Near Infrared Channels of the Advanced Very High Resolution Radiometer on NOAA-7,-9, and -11 Spacecraft. C. R. Nagaraja Rao and Jianhua Chen, April 1994.

NESDIS 79 Quality Control and Processing of Historical Oceanographic Nutrient Data. Margarita E. Conkright, Timothy P. Boyer and Sydney Levitus, April 1994.

NOAA SCIENTIFIC AND TECHNICAL PUBLICATIONS

The National Oceanic and Atmospheric Administration was established as part of the Department of Commerce on October 3, 1970. The mission responsibilities of NOAA are to assess the socioeconomic impact of natural and technological changes in the environment and to monitor and predict the state of the solid Earth, the oceans and their living resources, the atmosphere, and the space environment of the Earth.

The major components of NOAA regularly produce various types of scientific and technical information in the following kinds of publications:

PROFESSIONAL PAPERS - Important definitive research results, major techniques, and special investigations.

CONTRACT AND GRANT REPORTS - Reports prepared by contractors or grantees under NOAA sponsorship.

ATLAS - Presentation of analyzed data generally in the form of maps showing distribution of rainfall, chemical and physical conditions of oceans and atmosphere, distribution of fishes and marine mammals, ionospheric conditions, etc.

TECHNICAL SERVICE PUBLICATIONS - Reports containing data, observations, instructions, etc. A partial listing includes data serials; prediction and outlook periodicals; technical manuals, training papers, planning reports, and information serials; and miscellaneous technical publications.

TECHNICAL REPORTS - Journal quality with extensive details, mathematical developments, or data listings.

TECHNICAL MEMORANDUMS - Reports of preliminary, partial, or negative research or technology results, interim instructions, and the like.

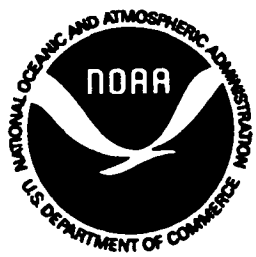

U.S. DEPARTMENT OF COMMERCE
National Oceanic and Atmospheric Administration
National Environmental Satellite, Data, and Information Service
Washington, D.C. 20233